Extracellular vesicles from early-stage *P. falciparum*-infected red blood cells contain PfEMP1 and induce transcriptional changes in human monocytes

Running title: *P. falciparum* vesicles have PfEMP1 and affect monocytes

Natália G. Sampaio[a,b], Samantha Emery[a,b], Alexandra Garnham[b,c], Qiao Y. Tan[a,b], Xavier Sisquella[b,d], Matthew A. Pimentel[b,d], Neta Regev-Rudzki[b,d], Louis Schofield[a,e], Emily M. Eriksson[a,b]

[a] Population Health and Immunity Division, Walter and Eliza Hall Institute of Medical Research, Parkville, Victoria, Australia

[b] Department of Medical Biology, University of Melbourne, Parkville, Victoria, Australia

[c] Bioinformatics Division, Walter and Eliza Hall Institute of Medical Research, Parkville, Victoria, Australia

[d] Infection and Immunity Division, Walter and Eliza Hall Institute of Medical Research, Parkville, Victoria, Australia

[e] Australian Institute of Tropical Health and Medicine, James Cook University, Townsville, Queensland, Australia

This article has been accepted for publication and undergone full peer review but has not been through the copyediting, typesetting, pagination and proofreading process which may lead to differences between this version and the Version of Record. Please cite this article as doi: 10.1111/cmi.12822

Corresponding author:

Emily M. Eriksson

The Walter and Eliza Hall Institute of Medical Research

1G Royal Parade, VIC 3052 Australia

Tel: +61 3 93452462, Fax: +61 3 93470852, email: eriksson@wehi.edu.au

Current affiliations:

NGS - Medical Research Council Human Immunology Unit, Radcliffe Department of Medicine, Medical Research Council Weatherall Institute of Molecular Medicine, University of Oxford, Oxford, UK

NRR - Department of Biomolecular Sciences, Weizmann Institute of Science, Rehovot, Israel

Summary

Pathogens can release extracellular vesicles (EVs) for cell-cell communication and host modulation. EVs from *Plasmodium falciparum*, the deadliest malaria parasite species, can transfer drug resistance genes between parasites. EVs from late-stage parasite-infected RBC (iRBC-EVs) are immunostimulatory and affect endothelial cell permeability, but little is known about EVs from early-stage iRBC. We detected the parasite virulence factor PfEMP1, which is responsible for iRBC adherence and a major contributor to disease severity, in EVs only up to 12 hours-post RBC invasion. Furthermore, using PfEMP1 transport knock-out parasites, we determined that EVs originated from inside the iRBC rather than the iRBC surface. Proteomic analysis detected 101 parasite and 178 human proteins in iRBC-EVs. Primary human monocytes stimulated with iRBC-EVs released low levels of inflammatory cytokines, and showed transcriptomic changes. Stimulation with iRBC-EVs from PfEMP1 knock-out parasites induced more gene expression changes, and affected pathways involved in defense response, stress response, and response to cytokines, suggesting a novel function of PfEMP1 when present in EVs. We show for the first time the presence of PfEMP1 in early-stage *P. falciparum* iRBC-EVs, and the effects of these EVs on primary human monocytes, uncovering a new mechanism of potential parasite pathogenesis and host interaction.

Introduction

The apicomplexan parasite *Plasmodium falciparum* caused 99% of the estimated 429,000 malaria deaths in 2015, predominantly affecting children in sub-Saharan Africa (WHO Malaria Report 2016). Mortality arises from severe disease complications such as anemia, metabolic acidosis, and cerebral malaria (White et al., 2014). *P. falciparum* invades red blood cells (RBC) and progresses through several distinct stages over a 48 hour asexual life cycle. After invasion, the parasite is surrounded by the parasitophorous vacuole, and is visualized as a ring in microscopy, hence named 'ring stage'. As the parasite develops inside the RBC, it enters the trophozoite stage, and then matures into a schizont prior to RBC rupture and parasite egress in the form of many invasive merozoites.

As the parasite progresses through the intraerythrocytic life cycle, the host cell is significantly altered. These changes are caused by the production and export of parasite proteins, of which many are inserted into the RBC plasma membrane; and by the introduction of parasite organelles, such as the Maurer's Clefts, into the RBC cytoplasm (Maier, Cooke, Cowman, & Tilley, 2009). A key parasite protein at the RBC surface is *Plasmodium falciparum* erythrocyte membrane protein 1 (PfEMP1). PfEMP1 binds to host cell surface molecules such as ICAM-1, CD36 and CSA, and causes iRBC sequestration in blood vessels and organs in order to avoid destruction in the spleen (Baruch, Gormely, Ma, Howard, & Pasloske, 1996; Reeder et al., 1999; Schofield & Grau, 2005). This adherence is a major contributor to *P. falciparum* pathogenesis, and can lead to particularly severe complications when sequestration occurs in blood vessels of the brain (Jensen et al., 2004; Tembo et al., 2014). Furthermore, PfEMP1 can dampen cytokine release from NK cells, γδ T cells

(D'Ombrain et al., 2007), and monocytes (Sampaio et al., 2017). PfEMP1 is produced early in the intraerythrocytic life cycle, already detectable in the parasite 8 hours post-invasion, and is shuttled through Maurer's Clefts to appear at the iRBC surface from 16 hours post-invasion (Kriek et al., 2003; McMillan et al., 2013). As a result, cytoadherence of the iRBC occurs when parasites are in the trophozoite stage, but early ring-stage parasites remain in circulation.

There have been increasing investigations into the role of extracellular vesicles (EVs) in malaria biology and pathogenesis (recently reviewed here (Sampaio, Cheng, & Eriksson, 2017)). EVs are bi-lipid membrane vesicles that are released from cells, either by budding from the plasma membrane or by generation and release of intravesicular bodies. They generally contain proteins and nucleic acids, and can fuse or be endocytosed by other cells. Mouse models of *Plasmodium* infection showed that parasite-derived EVs can induce an immune response (Couper et al., 2010; Martin-Jaular, Nakayasu, Ferrer, Almeida, & Del Portillo, 2011). Similarly, EVs from late-stage trophozoite/schizonts, can induce an inflammatory response from human monocytes/macrophages (Mantel et al., 2013) and can modulate epithelial cell gene expression and barrier properties (Mantel et al., 2016). Furthermore, *P. falciparum* iRBC-derived EVs allow cell-cell communication between parasites, and EVs from ring-stage iRBC were particularly efficient at parasite-to-parasite gene transfer (Mantel et al., 2013; Regev-Rudzki et al., 2013). However, the study of EVs from the early ring-stage of the asexual lifecycle has been limited. Therefore, we aimed to investigate this population of vesicles and examine the effect of EVs on host innate immune cells.

We hypothesized that ring-stage iRBC would release vesicles with unique characteristics, and that these could stimulate host monocytes. We analysed EVs from iRBC at different life stages, and found that the protein content of EVs changed over time. Intriguingly, we discovered that the key *P. falciparum* virulence factor PfEMP1 was present only in EVs from early ring-stage parasites, many hours before PfEMP1 appearance on the iRBC surface, providing a means of the parasite to disseminate PfEMP1 early in infection. Furthermore, these ring-stage EVs induce low level cytokine responses from human primary monocytes, while altering the cellular transcriptome. The EV effects on gene expression were partially PfEMP1-dependent, suggesting a role for EV-delivered PfEMP1 in modulating the host immune response to infection.

Results

Extracellular vesicles from early-stage iRBC contain the virulence factor PfEMP1

To investigate the potential changes in the protein content of EVs released during the parasite life cycle, vesicles were obtained from iRBC (iRBC-EVs) at different stages of maturity. Wild type CS2 iRBC were tightly synchronised to a 4-hour window, and vesicles were isolated in 12 hour increments, i.e. at 12, 24, 36 and 48 hours post-invasion, representing ring, early trophozoite, late trophozoite and schizont stages (Figure 1A). The iRBC-EVs from the four different stages were analysed by Western blot for the presence of *P. falciparum* proteins PfEMP1, Plasmepsin V, aldolase, and actin depolymerisation factor (ADF1). PfEMP1 is a key

virulence factor, and EVs derived from ring stage iRBC contained PfEMP1, whereas PfEMP1 was absent in EVs after 12 hours (Figure 1B). Notably, PfEMP1 is reported to appear on the iRBC surface from 16 hours post-invasion and peak at 36 hours post-invasion (Kriek et al., 2003), and we confirmed this timing with iRBC lysates at the indicated 12 hour intervals (Figure 1C). PfEMP1 is therefore present in iRBC-EVs significantly earlier than it's expression on the iRBC surface. The levels of other parasite proteins in iRBC-EVs also varied at different life-stages. Parasite aldolase, an actin-binding protein involved in parasite invasion and motility (Diaz et al., 2014), was found at high levels in both ring stage and schizont-stage iRBC-EVs, whereas parasite ADF1, another actin-binding protein (Wong et al., 2014), was abundant in iRBC-EVs from the schizont-stage (Figure 1B). SR1 is a RBC protein and known marker of erythrocyte-derived vesicles (Salzer, Hinterdorfer, Hunger, Borken, & Prohaska, 2002), and was used to demonstrate equivalent loading of all samples. Thus, we find that parasite proteins in iRBC-EVs vary throughout the parasite life cycle, and that PfEMP1 is present only in EVs from early ring-stage iRBC.

PfEMP1 presence in extracellular vesicles is independent of transport proteins SBP1 and PTP1

The transport of PfEMP1 from the parasite within the parasitophorous vacuole to the iRBC plasma membrane is a regulated process involving many parasite proteins (Maier et al., 2009). Genetic ablation of key proteins in this transport pathway, such as skeletal binding protein 1 (SBP1), or PfEMP1 transport protein 1 and 2 (PTP1 and PTP2), results in PfEMP1 being expressed but localized in the parasite or parasitophorous vacuole rather than the iRBC plasma membrane (Cooke et al., 2006; Maier et al., 2007; Maier et al., 2008). EVs from CS2-SBP1-KO, CS2-

PTP1-KO and CS2-PTP2-KO iRBC were analysed for the presence of PfEMP1. iRBC-EVs from both CS2-SBP1-KO and CS2-PTP1-KO still contained PfEMP1, whereas PfEMP1 expression was negligible both CS2-PTP2-KO iRBC and iRBC-EVs (Figure 2A). However, parasite aldolase and ADF1 were still detected in EVs from CS2-PTP2-KO iRBC. Thus, SBP1 and PTP1 are not required for PfEMP1 incorporation into EVs, or EV release from iRBC. This data suggests that the EVs originate from the intracellular parasite rather than budding from the RBC membrane, as vesicles budding from the membrane of CS2-SBP1-KO or CS2-PTP1-KO iRBC would not contain PfEMP1.

Proteomic analysis of iRBC-EVs allowed quantitative discovery of parasite and human proteins in EVs

In order to investigate the potential downstream effects of PfEMP1 in iRBC-EVs, we first performed an in-depth analysis of the proteins present in EVs from ring-stage wild type 3D7 (3D7-WT) and the 3D7-UpsC^{R} PfEMP1 knock-out parasite strain. The 3D7-UpsC parasite contains the h*dhfr* gene, which confers resistance to WR99210, downstream of the UpsC PfEMP1 promoter (Voss et al., 2006). Due to the allelic exclusivity of PfEMP1 expression, where only one PfEMP1-encoding gene is expressed at a time, the 3D7-UpsC^{R} does not express PfEMP1 in the presence of WR99210. Western blot analysis confirmed that PfEMP1 was present in iRBC-EVs from ring-stage 3D7-WT and absent in those from 3D7-UpsC^{R} (Figure 2B). To determine if proteins other than PfEMP1 were also differentially expressed in the iRBC-EVs from 3D7-UpsC^{R} compared to 3D7-WT, label-free, quantitative proteomics of EV proteins was performed. To obtain highly purified iRBC-EVs, culture supernatant was fractionated by Optiprep density centrifugation (Van Deun et al.,

2014). Western blot for *P. falciparum* aldolase and exosome marker flotilin-1 indicated that EVs were enriched in fractions 7 and 8 (Figure 3A). The density of these fractions was 1.10-1.12 g/ml (Figure 3B), which corresponds to the expected range for exosomes (Tauro et al., 2012). Fractions 7 and 8 from 3D7-WT and 3D7-UpsC^{R} were pooled and three independent biological replicates were processed for mass spectrometry.

Peptides detected by mass spectrometry were searched separately against both human and *P. falciparum* databases and low stringency hits were determined. A total of 178 human proteins and 101 parasite proteins were identified (Table 1 and S1). PfEMP1 could not be reliably identified in these data sets, despite being identified by Western blot analysis. When the label-free quantitative (LFQ) intensity measurements of human and *Plasmodium* proteins were compared to intensities of proteins from the Maxquant contaminant database, *Plasmodium* proteins were predominately of lower abundance while contaminant proteins (e.g. serum albumin) dominated higher abundance proteins (Figure S1). As a result, vesicle proteins were less likely to be sampled for MS/MS and more likely to be below detection limits, which are the likely explanations for non-detection of PfEMP1. Other parasite proteins of interest that were reliably identified by proteomics include merozoite surface protein 1 (MSP-1), knob-associated histidine-rich protein (KHARP), PfEMP3, and stevor (Table S1). Furthermore, the exosome marker flotilin-1 and *P. falciparum* aldolase, which were detected by Western blot analysis, were reproducibly identified by proteomics.

The gene ontology (GO) annotations for proteins were downloaded from UniProt databases for human and *Plasmodium* (Table S2). Similarities in

overarching molecular function of human and malaria proteins in iRBC-EVs included 'Endopeptidase Activity' and 'ATP Binding' as the most abundant functions in both datasets (Figure 3C). In contrast, proteins with functions in 'Structural Constituent of Ribosomes', 'GTPase Activity', 'Histone Binding', and 'Structural Constituent of Cytoskeleton' were overrepresented in parasites proteins but not human. Moreover, 'Serine-type Endopeptidase', 'Heme/Oxygen/Iron Binding', 'Cadherin Binding', and 'Receptor Binding' functions were overrepresented in human proteins only. Additionally, the 'Extracellular Exosome' GO annotation for cellular compartment was also enriched in the human protein dataset (Table S2). Network analysis using the STRING database (Szklarczyk et al., 2017) showed protein interactions, and highlighted clusters for 'Proteasome-associated Proteins' for both *Plasmodium* and human data sets (Figure 3D). 'Robosomal Proteins', 'Rhoptry/Antigen' and 'Membrane/Antigen' protein interaction clusters are present for *Plasmodium* proteins, whereas 'Complement/Protease', 'Erythrocyte Membrane', 'Hemoglobin-binding Proteins' and 'Flotillin' clusters are present for human proteins, highlighting functional differences in the two data sets.

Quantitative analysis of protein abundance between 3D7-WT and 3D7-UpsC^{R} iRBC-EVs was performed using LFQ intensities for reproducibly identified proteins via a two-sample t-test. For proteins with a significant p-value (<0.05) the difference between means was also assessed, which demonstrated the majority of statistically significant proteins were not accompanied by large changes in abundance (Table S3, Figure 3E). Of the statistically significant, differentially expressed proteins (Table 2), one human protein (Histone H2B) and no parasite proteins found to be above the cut-off log-transformed mean difference of 2. Furthermore, several proteins were reproducibility identified exclusively in one treatment group but were not detected in

any replicate of the other, and could not be means tested. Four *Plasmodium* and seven human proteins were detected exclusively in 3D7-UpsC^{R} iRBC-EVs, whereas two human proteins only detected in 3D7-WT iRBC-EVs (Table S4). These proteins could be of low abundance and below detection limits (Figure S1), or could represent biological differences between groups.

Extracellular vesicles from ring-stage iRBC are less immunostimulatory than whole trophozoite iRBC

Mantel et al. (Mantel et al., 2013) reported that CD14+ monocytes were the main immune cell population targeted by iRBC-EVs, and that monocyte-derived macrophages stimulated with EVs from late-stage iRBC upregulated the expression of IL-1β, IL-6, IL-10 and IL-12, and released IL-10 and TNF. However, the response to ring stage iRBC-EVs was not evaluated. We have recently shown that PfEMP1 located on the iRBC surface can specifically modulate the monocyte immune response to parasites (Sampaio et al. 2017). However, to investigate whether the presence of PfEMP1 in ring stage iRBC-EVs had a similar effect on monocytes, the optimal EV concentration for cell stimulation was first determined by flow cytometry to achieve the highest response (iRBC-EV) to background (uRBC-EV) signal (Figure S2). The cytokine and chemokine production from primary human monocytes in response to iRBC-EVs from ring-stage 3D7-WT and 3D7-UpsC^{R} was subsequently assessed. Furthermore, the magnitude of the cytokine response was compared to whole trophozoite-stage iRBC, in order to provide a reference for cytokine responses to known immunostimulatory parasites within the same donor.

Primary human monocytes from five donors were co-incubated for 12 hours with 5 µg/ml of uRBC-EVs or iRBC-EVs from ring-stage 3D7-WT or 3D7-UpsC^{R}, or

intact uRBC or 3D7-WT trophozoite iRBC. Levels of released IL-1β, IL-6, IL-10, IL-12p40, MCP-1, MIP-1α, MIP-1β and TNF, cytokines commonly associated with monocyte responses to malaria (Stanisic et al., 2014), were measured by multiplex cytokine ELISA (Figure 4). As previously observed for human PBMC stimulations with *P. falciparum*, the range of cytokine responses varied from donor to donor (D'Ombrain et al., 2008; Stanisic et al., 2014). Some donors had consistently high cytokine responses to both iRBC-EVs and trophozoites, whereas others did not respond to iRBC-EVs at all (Figure 4). There were significantly more IL-12p40, MCP-1, and MIP-1β released in response to trophozoites compared to iRBC-EVs, but no differences were seen between stimulation with iRBC-EVs from 3D7-WT versus 3D7-UpsC^{R} parasites. Overall, this data showed that iRBC-EVs from early ring-stage induce low or no cytokine responses from the majority of human donors, but high donor heterogeneity exists.

Ring-stage-derived extracellular vesicles induce transcriptional changes in human monocytes that are partially PfEMP1 dependent

Although the monocyte cytokine responses to iRBC-EVs were relatively low, the transcriptional profile of these cells in response to EVs was assessed. Primary human monocytes from six donors were stimulated with EVs from ring-stage 3D7-WT, 3D7-UpsC^{R}, or uRBC for six hours followed by RNA. RNA-sequencing was used to measure transcriptional changes in monocytes in response to EV treatments. Median of 23 million reads (min 16, max 64 million) were obtained for each sample, and >90% of reads were successfully mapped to the human genome. No sequences mapped to the *Plasmodium falciparum* genome. After filtering, 10,123 genes were classified as expressed in at least one biological condition as

determined by filtering criteria (see methods). A multi-dimensional scaling (MDS) plot shows samples clustering according to stimulation (Figure 5A).

Differential expression of genes in monocytes stimulated with uRBC-EVs, 3D7-WT iRBC-EVs or 3D7-UpsC^{R} iRBC-EVs was determined, with a 5% false discovery rate (Figure 5B and C). There were 181 differentially expressed (DE) genes in monocytes stimulated with 3D7-WT iRBC-EV compared to uRBC-EVs, whereas there were 530 DE genes when cells were stimulated with 3D7-UpsC^{R} iRBC-EVs (Figure 5B, Table 3 and S5). There was no statistically significant difference in gene expression when cells were stimulated with vesicles from 3D7-WT compared to 3D7-UpsC^{R}. Nevertheless, heatmaps depicting the up- or downregulation of genes in each donor with the different EV stimulations indicated a trend in gene expression changes between monocytes incubated with 3D7-WT and 3D7-UpsC^{R} iRBC-EVs (Figure 5E). This shows that overall gene expression in monocytes following stimulation with iRBC-EVs compared to uRBC-EVs causes significant changes, but that the differences between response to 3D7-WT and to 3D7-UpsC^{R} iRBC-EVs are more subtle. Notably, there were 2.9-fold more DE genes in cells stimulated with 3D7-UpsC^{R} iRBC-EVS versus 3D7-WT iRBC-EVs, compared to uRBC-EV stimulus, indicating that monocytes had a consistently greater response to 3D7-UpsC^{R} iRBC-EVs.

There was some overlap between the DE genes in monocytes stimulated with iRBC-EVs from 3D7-WT compared to 3D7-UpsC^{R} (Figure 5D). Of the 181 DE genes in 3D7-WT iRBC-EV treatment, 143 (79%) were also changed in 3D7-UpsC^{R}. In comparison, only 27% of DE genes in 3D7-UpsC^{R} iRBC-EV-stimulated were also changed in 3D7-WT iRBC-EV-stimulated cells. However, nearly half of the top

twenty most differentially expressed genes in both treatments were the same (Table 4). The majority of these common DE genes are involved in transcription/translation, and all were upregulated in both sample sets. As there were minimal changes in protein content of iRBC-EVs from 3D7-WT versus 3D7-UpsC^{R}, with the exception of PfEMP1, it is possible that differences in monocyte transcriptional changes between the two stimulations were due to PfEMP1 presence/absence.

Pathway analysis of gene expression changes in monocytes treated with iRBC-derived extracellular vesicles

In order to characterize the functional differences in the effect of monocyte stimulus with 3D7-WT and 3D7-UpsC^{R} iRBC-EVs, the GO pathways enriched in each data set were inferred (Table 5 and S6). Of the twenty most highly associated GO terms in the iRBC-EV stimulated samples, ten were common between the two treatments. In addition to transcription/translation processes, there was an enrichment of GO terms related to cellular metabolism/catabolism. Of interest are the enriched GO terms that were not in common between the two treatments. These included ‘defense response’, ‘cellular response to cytokine stimulus’, and ‘response to stress’ enriched only with 3D7-UpsC^{R} iRBC-EV stimulus, and not with 3D7-WT iRBC-EVs. In addition, there was enrichment of terms involving antigen presentation in both treatment groups.

Type I interferons were recently found to be released in response to human malaria infection, but to suppress immunity to the infection (Montes de Oca et al., 2016). To determine if there was an effect on genes specifically associated with interferon response, DE genes were searched against the Interferome database. Of the 181 DE genes induced by 3D7-WT iRBC-EVs, 30 were interferon response

genes (16.5%), and of the 530 DE genes induced by 3D7-UpsCR iRBC-EVs, 79 were interferon response genes (14.9%). In comparison, of the 10,123 genes in the data set, 1,182 were identified as interferon response genes (11.6%). This suggests that treatment of monocytes with iRBC-EVs could elicit a type I interferon response signature.

Discussion

Extracellular vesicles are increasingly being recognised to play important roles in parasite cell-cell communication and interaction with the host (Mantel & Marti, 2014; Sampaio et al., 2017). Many parasite species produce EVs and employ these for modulation of host cells, which enhances pathogenesis (Szempruch et al., 2016; Twu et al., 2013) and/or inhibits immune responses (Buck et al., 2014; Silverman et al., 2010). The discovery that *P. falciparum* can use EVs for intra-parasite communication and exchange of genetic information (Mantel et al., 2013; Regev-Rudzki et al., 2013) has revealed a new aspect of parasite biology and potential host interactions. We investigated EVs from early ring-stage iRBC, and found that these vesicles contain PfEMP1 and induce transcriptional changes in human monocytes.

PfEMP1 is a transmembrane protein that is a key virulence factor in *P. falciparum* malaria, largely responsible for the enhanced pathogenesis and mortality associated with this disease (Miller, Baruch, Marsh, & Doumbo, 2002). We demonstrated that PfEMP1 is present in a novel parasite compartment, and may affect the host response to infection. The protein content of *P. falciparum* iRBC-EVs differed throughout the parasite life cycle, notably with the presence of PfEMP1 in EVs released only from early ring-stage iRBC. Of note, the limited timeframe in

which PfEMP1 was observed in EVs was different from the appearance of PfEMP1 at the iRBC plasma membrane. PfEMP1 trafficking occurs through intracellular vesicles moving from the parasite to the cell membrane, via the Maurer's clefts, (McMillan et al., 2013). It is conceivable that the PfEMP1-containing EVs studied here were released as a byproduct of PfEMP1 transport to the RBC surface. However, PfEMP1 is only present in EVs in the first 12 hours post-invasion, whereas the intracellular transport of PfEMP1 still occurs after 12 hours, indicating the processes are temporally distinct. Therefore, it is unlikely that the intracellular PfEMP1-trafficking vesicles correspond to the EVs studied here. This suggests that the inclusion of PfEMP1 in EVs could be a specific mechanism applied by the parasite to affect host cells.

EVs from late-stage iRBC contain miRNA that can downregulate target genes in endothelial cells to affect barrier function (Mantel et al., 2016). Since PfEMP1 can interact with a variety of host cell receptors and dampen cytokine responses from innate immune cells, it is possible that delivery of PfEMP1 via EVs could provide an additional means of host manipulation. Alternatively, PfEMP1 could be deployed in EVs early during parasite infection as a decoy antigen. Indeed, *Trypanosoma cruzi* employ EVs as a decoy for complement attack (Cestari, Ansa-Addo, Deolindo, Inal, & Ramirez, 2012; Díaz Lozano et al., 2017), and exosomes have also been implicated in evasion of humoral immunity in cancer (Aung et al., 2011). A significant proportion of the natural antibody immunity against *P. falciparum* targets PfEMP1 (Bull et al., 1998), and *P. falciparum* EVs can be detected by serum from malaria-infected patients *in vitro* (Mantel et al., 2013). Hence, PfEMP1-containing EVs could serve to attract neutralizing antibodies to protect the parasite against targeted

immune attack. It would be interesting to evaluate whether parasite EVs from malaria-infected patients bind parasite-specific antibodies *in vivo*.

Although we did not directly investigate the origin of iRBC-EVs, these vesicles were enriched for the exosome marker flotilin-1, and proteins detected in iRBC-EVs by proteomics were highly associated with the exosomal cell compartment according to gene ontology analysis. This suggests that these iRBC-EVs could be exosomes, or at least originate from within the parasite, rather than being microvesicles shed from the iRBC plasma membrane. This is further supported by use of PfEMP1 transport knockout parasites, which express PfEMP1, but lack PfEMP1 on the iRBC surface (Maier et al., 2007; Maier et al., 2008). PfEMP1 was present in iRBC-EVs from these knockout parasites indicating that iRBC-EVs originated from the intracellular parasite and were released through a still unknown mechanism. Moreover, another study of *P. falciparum*-derived microparticle/microvesicles, which are large vesicles derived from the iRBC plasma membrane, showed that these contain the parasite ring-infected erythrocyte surface antigen (RESA), which we did not detect in our iRBC-EVs (Nantakomol et al., 2011), further distinguishing them from the more widely investigated surface-derived microparticles. Further studies are needed to determine whether the iRBC-EVs are exosomes, or microvesicles/microparticles from the parasite plasma membrane or from parasite-derived RBC organelles such as Maurer's Clefts.

Mass spectrometry of iRBC-EVs from 3D7-WT and 3D7-UpsC^{R} parasites provided the first in-depth analysis of the protein content of ring-stage iRBC-EVs. Using this method, we detected more peptides than previous proteomic analysis of *P. falciparum* iRBC-EVs (Mantel et al., 2013). In addition, label-free quantitative

proteomics provided an unbiased comparison of the protein abundance between 3D7-WT and 3D7-UpsC^{R} vesicles. Overall, there was little difference in the quantity of proteins in iRBC-EVs from both strains, though it is possible that differences in low abundance proteins were not detected by proteomics. Technologies to deplete contaminating proteins from the sample could allow better resolution of lower abundance parasite proteins. There were similarities between the protein content detected in early-stage iRBC-EVs and that reported for late-stage iRBC-EVs (Mantel et al., 2013). Parasite proteins MSP-1, Rhop2, HSP-70, GAPDH, CLAG3.1, Ef1-alpha were among the top twenty proteins identified in both studies, consistent with their expression patterns throughout the parasite life cycle (Llinás, Bozdech, Wong, Adai, & DeRisi, 2006). PfEMP1 was not reported in EVs from trophozoites/schizonts (Mantel et al., 2013), in agreement with our finding that PfEMP1 is only present in early ring-stage iRBC-EVs. The function of the various parasite proteins identified in iRBC-EVs is still largely unknown, and thus further investigations are needed to understand their role in EVs.

Human primary monocytes were chosen as the target cell population for investigation of early-stage iRBC EV effects, since these were the primary responders to EVs from late-stage iRBC (Mantel et al., 2013). Although ring-stage iRBC-EVs were less stimulatory than intact trophozoite iRBC, there was still a cytokine response to iRBC-EVs. The main pro-inflammatory agonists from iRBC that are detected by monocytes are GPI and hemozoin, which stimulate TLRs and inflammasomes (Eriksson, Sampaio, & Schofield, 2013; Gazzinelli, Kalantari, Fitzgerald, & Golenbock, 2014). The presence of GPI in iRBC-EVs has not been investigated, but given that many parasite proteins are GPI-anchored (e.g. MSP-1) it is plausible that GPI is present in iRBC-EVs. Moreover, there were high peptide

counts from heat shock proteins (Hsp) in our proteomic analysis of ring-stage iRBC-EVs. Hsp are important in parasite survival and adaptation to hostile environments, and are exported to the iRBC cytoplasm during infection (Shonhai, Boshoff, & Blatch, 2007). Indeed, Hsp70 is a danger signal known to be enriched in EVs from other species (De Maio, 2011), and Hsp70 in EVs can activate innate immune cells (Gastpar et al., 2005; Lv et al., 2012; Vega et al., 2008). The heat shock proteins in iRBC-EVs could be detected as danger signals, and thus induce monocyte activation. Conversely, EVs used in this work did not contain hemozoin, as this was removed during the EV isolation process. The lack of proinflammatory hemozoin, and the overall lower quantities of parasite agonists, supports the observed low capacity of ring-stage iRBC-EVs to stimulate innate immunity. Thus, these EVs may predominantly provide the parasite with a means of cell-cell communication that has minimal interference from host immune cells. It is important to note, however, that some donors were able to respond to iRBC-EVs, indicating that natural variations in human innate responses likely play a role in detection of ring-stage iRBC-EVs.

By using transcriptomics to study monocyte gene expression changes in response to ring-stage iRBC-EVs, we further dissected the effect of these vesicles on human monocytes and the contribution of PfEMP1 in this response. The transfer of antigens from extracellular vesicles to antigen presenting cells for T cell priming has been extensively demonstrated (Beauvillain, Ruiz, Guiton, Bout, & Dimier-Poisson, 2007; Robbins & Morelli, 2014). The upregulation of antigen presentation pathways after stimulation with iRBC-EVs indicates that monocytes can not only sense these EVs but also take up antigens for presentation. Additionally, there was an enrichment of interferon response genes among the genes differentially expressed with iRBC-EV treatment, which could be relevant to the recent discovery

that type I interferons suppress innate and adaptive immunity to *P. falciparum* infection in humans (Montes de Oca et al., 2016). Nevertheless, there was a difference in monocyte transcriptome changes when cells were stimulated with PfEMP1-positive or PfEMP1-negative iRBC-EVs. Namely, stimulus with PfEMP1-negative iRBC-EVs induced nearly three-fold more gene expression changes compared to PfEMP1-positive iRBC-EVs, and upregulated pathways involving 'defence response', 'cellular response to cytokine stimulus', and 'response to stress', which were not upregulated with the PfEMP1-positive iRBC-EVs. PfEMP1, when in the biologically relevant concentrations and cellular localization of the iRBC surface, inhibits monocyte responses (Sampaio et al. 2017). It is possible that PfEMP1 could also exert an immune modulatory effect on monocytes when delivered via EVs. Hence, PfEMP1 might not affect EV uptake by monocytes, but could potentially manipulate monocyte responses to stimulus, as is seen with PfEMP1 on the iRBC surface. However, further work is still required to unequivocally demonstrate this effect.

Recent reports have shown that EVs from late-stage iRBC contain RNA. Since ring-stage iRBC-EVs can provide a means of exchange of genetic material, then these vesicles must also contain nucleic acids. Therefore, nucleic acids in ring-stage iRBC-EVs could also account for transcriptional changes in monocytes. Although we did not detect parasite RNA in monocytes treated with iRBC-EVs, it is possible that parasite nucleic acids were delivered to host cells but degraded prior to RNA extraction. Studies into the nucleic acid content of ring-stage iRBC-EVs, and their effects on host cells, are needed in order for the function of these vesicles to be completely understood.

The work presented here demonstrates that EVs from early-stage *P. falciparum*-infected RBC affect host monocytes, modifying gene expression while inducing low cytokine secretion. As there have been numerous examples that pathogen-derived EVs can modulate host cells in order to inhibit the immune response and promote pathogen survival, *P. falciparum* might employ EVs for similar outcomes. These findings could have important implications for our understanding of parasite modulation of host immunity, and warrant further investigation into the breadth and magnitude of their effects.

Materials and Methods

Parasite culturing

Reagents were purchased from Sigma-Aldrich unless otherwise specified. Parasites were maintained in RPMI-1640 medium pH 7.4, 25 mg/ml HEPES, 50 µg/ml hypoxanthine, 2 mg/ml sodium bicarbonate, 20 µg/ml gentamycin, supplemented with 5% human serum and 0.25% AlbumaxII. Parasites were grown in pooled donor red blood cells (RBC;) provided by the Australian Red Cross at 4% hematocrit, and incubated at 37°C in 1% O_2, 4% CO_2 and 95% N_2. Wild type parasite strains used were 3D7 and CS2. PfEMP1 knockdown 3D7-UpsC^R (Voss et al., 2006), and CS2 parasites with the disrupted SBP-1 (PF3D7_0501300), PTP-1 (PF3D7_0202200, PFB0106), and PTP-2 (PF3D7_0731100, MAL7P1.172) genes, referred to respectively as CS2-SBP1-KO, CS2-PTP1-KO, and CS2-PTP2-KO, were kindly provided by Alan Cowman (Maier et al., 2007; Maier et al., 2008). 3D7-UpsC^R parasites cultured in the presence of 4 mg/ml blasticidin-S and 4 nM WR99210, do

not express PfEMP1 (Voss et al., 2006). Cultures were routinely screened for mycoplasma contamination using MycoAlert Plus Kit (Lonza).

Knob-expressing parasites were selected for by gelatin flotation fortnightly (Goodyer, Johnson, Eisenthal, & Hayes, 1994). Parasite cultures were synchronized by treating ring-stage parasites with 5% sorbitol solution at 37°C for 10 min to lyse trophozoite/schizont-stage parasites. For tight synchronization, parasites were grown until schizont stage, magnet purified by cell sorting on CS columns (Miltenyi Biotec), and added to fresh uRBC in culture medium for up to 4 hr to allow invasion, then remaining trophozoites/schizonts were lysed using 5% sorbitol (McMillan et al., 2013). For cell stimulations, magnetic cell sorted iRBC were used.

Isolation of iRBC vesicles

Parasites or uRBC were grown in 0.5% AlbumaxII for 12 hr, unless otherwise indicated, and culture medium was collected for vesicle isolation. Vesicles were isolated as described previously (Lässer, Eldh, & Lötvall, 2012). Briefly, cells and cellular debris (e.g. hemozoin) were removed by sequential centrifugation at 300 x g for 5 min, and 3000 x g for 10 min. Large vesicles, cellular organelles, and debris were further removed by passing supernatant through 0.2 µm filter (Sartsted). Vesicles were pelleted by ultracentrifugation in H_2O_2-treated Optiseal tubes (Beckman Coulter) at 120,000 x g overnight at 4°C in a Ti70 rotor, re-suspended in 25 ml of PBS and ultracentrifuged at 120,000 x g for 4 hr at 4°C. Vesicle pellets were re-suspended in 50-100 µl of PBS and maintained on ice, or stored at -80°C. A flow chart of vesicle preparation and usage is show in Figure S3. For cell stimulation assays, freshly isolated vesicles were used. Protein concentrations were determined using BCA assay (Pierce) according to manufacturer's instructions.

SDS-PAGE and Western Blotting

Samples were solubilized with NuPAGE LDS sample buffer, reduced with 2-mecraptoethanol, and analyzed on 3-8% Tris-Acetate gels (for PfEMP1 visualization) or 4-12% Bis-Tris gels (NuPAGE, Thermo Fisher Scientific) and transferred to nitrocellulose (Criterion, Bio-Rad) according to manufacturer's instructions. Membranes were blocked with 5% BSA, 0.05% NP-40 Tris-buffered saline (TBS) and probed with anti-Pf Aldolase (Baum et al., 2006), anti-PfEMP1-ATS (clone 1B/98-6H1-1), anti-Plasmepsin V (Boddey et al., 2010), anti-Pf ADF1/cofilin (Wong et al., 2011), anti-SR1/sorcin (Abcam), or anti-flotillin (BD biosciences), and HRP-conjugated anti-mouse or anti-Rabbit IgG antibody (Cell Signaling Technology) in 0.5% milk, 0.05% NP-40 TBS.

Proteomics

Culture medium from early ring-stage parasites cultured for 12 hr (40 ml, 4% haematocrit, 8% parasiteamia) was centrifuged at 3000 x g for 10 min and filtered through a 0.2 µm syringe filter. Samples were concentrated to 1 ml by centrifugal filtration using Vivaspin 20 Polyethersulfone 100,000 MWCO tubes (Sartorius) and fractionated by density using discontinuous Optiprep gradients (Van Deun et al., 2014). Columns were centrifuged in SW40Ti rotor at 100,000 x g for 18 hr at 4°C. Twelve 1 ml fractions were collected and density of fractions was measured using a refractometer (Metler Toedo). Fractions were diluted in PBS, and centrifuged in 70 Ti rotor at 120,000 x g for 4 hr. Pellets were re-suspended using NuPAGE LDS sample buffer, and stored at -20°C.

EV protein was solubilized in 2.5% SDS in 100mM Tris (pH 8), reduced with 10mM DTT followed by alkylation with 15mM IAM. Proteins were precipitated by methanol-chloroform (Wessel & Flügge, 1984), re-solubilized in 8M Urea in 100mM Tris (pH 8) and protein concentration equalized across samples (BCA assay; Pierce). Protein was digested overnight with Trypsin (Promega) at 37°C (1µg enzyme to 100µg protein). Samples were acidified with 1% trifluoracetic acid and desalted using solid phase extraction (SPE) with tips packed with styrene divinyl benzene (3M Empore), and fractionated into three fractions as described (Rappsilber, Mann, & Ishihama, 2007). Extracts were dried by vacuum centrifugation, and reconstituted in 2% acetonitrile, 0.1% trifluoroacetic acid for nanoflow liquid chromatography tandem mass spectrometry (Nano LC-MS/MS).

Samples were analysed by LC-MS/MS using Orbitrap Lumos mass spectrometer (Thermo Scientific) fitted with nanoflow reversed-phase-HPLC (Ultimate 3000 RSLC, Dionex). The nano-LC system had an Acclaim Pepmap nano-trap column and Pepmap RSLC analytical column (Dionex – C18, 100 Å, 75 µm × 2 cm and 75 µm × 50 cm, respectively). 1 µL of the peptide mix was loaded at an isocratic flow of 5 µL/min of 3% CH_3CN containing 0.1% formic acid for 6 min before the enrichment column was switched in-line with the analytical column. The eluents used for the LC were 5% DMSO/0.1% v/v formic acid (solvent A) and 100% CH_3CN/5% DMSO/0.1% formic acid v/v. The gradient used was 3% B to 22% B for 29 min, 22% B to 40% B in 10 min, 40% B to 80% B in 5 min and maintained at 80% B for the final 5 min before equilibration for 10 min at 3% B prior to the next analysis.

The mass spectrometer was operated in positive-ionization mode (spray voltage 1.9 kV, source temperature 275°C). Lockmass of 401.92272 from DMSO

was used. Data-dependent acquisition mode MS spectra scanning from m/z 350-1550 at 120000 resolution with AGC target of $5e^5$ was used. The "top speed" acquisition method mode (3 sec cycle time) on the most intense precursor was used whereby peptide ions with charge states ≥2-5 were isolated with isolation window of 1.6 m/z and fragmented with high energy collision (HCD) mode with stepped collision energy of 30 ±5%. Fragment ion spectra were acquired in Orbitrap at 15000 resolution. Dynamic exclusion was activated for 30s.

Database searching was performed using MaxQuant (version 1.5.5.1) for label-free quantification (LFQ) (Cox & Mann, 2008; Tyanova, Temu, & Cox, 2016), using the PlasmoDB 3D7 protein coding sequence file (Aurrecoechea et al., 2009) for parasite proteins, and human proteins were searched against reviewed protein entries from UniProt. Default parameters were used for target and decoy searching with a false discovery rate (FDR) of 1% imposed for peptide-to-spectrum matches, and the LFQ minimum ratio count set to 1 and matching between runs set to 'match from and to'. Oxidation of methionine and N-acetylation of proteins' N-termini were set to variable modifications and carbidomethylation of cysteine was considered fixed modification. The Maxquant output file was imported in Perseus (Tyanova, Temu, Sinitcyn, et al., 2016) (version 1.5.5.3) and proteins/protein groups identified in the reverse database, contaminant database or only by site were removed. Low stringency proteins were filtered to detection in a minimum of three replicates across the six replicates of both treatment groups. For statistical analyses, high stringency proteins were filtered to only include those reproducibly identified in all three biological replicates within at least one sample group.

Gene ontology (GO) functions were obtained from Uniprot for non-homologous proteins from human and *Plasmodium*, and GO annotations for molecular function were used for further analysis. Network analysis was performed by submitting the UniProt ascensions to the STRING (Search Tool for the Retrieval of Interacting Genes) software (v10.5; http://string.db.org) (Szklarczyk et al., 2017). Interaction networks were visualised for proteins with medium confidence (0.4) with network edges based on evidence, with continuous lines for direct interactions and interrupted lines for indirect interactions. Clustering was based on a MCL algorithm inflation default parameter of 3.

Flow cytometric optimization of EV concentration for cell stimulation

Cryopreserved human PBMCs from naïve Melbourne donors were stimulated with 1, 5 or 10 µg/ml exosomes for 12 hrs at 37°C in 5% CO_2. Brefeldin A (10 µg/ml; Sigma, St Louis, MO) and GolgiStop (2µM; BD Biosciences, San Jose, CA) were added for the final 8 hrs of incubation. Cells were incubated for 10 min on ice with PBS containing 10mM glucose and 3mM EDTA to detach adherent cells. PBMCs were surface stained in FACS buffer (PBS containing 0.5% bovine serum albumin and 2 mM EDTA) on ice for 30 min with allophycocyanin-Cy7 (APC-Cy7)-conjugated anti-CD14 (clone MΦP9, BD Biosciences). Aqua live/dead amine reactive dye (Invitrogen) was used for dead cell exclusion. Cells were fixed in 2% paraformaldehyde and permeabilized using Permeabilizing solution 2 (BD Biosciences). Intracellular staining with Alexa700-conjugated anti-TNFα (clone MAb11; BD Biosciences), PE-conjugated anti-MIP1α (clone 93342; RnD Systems, Minneapolis MN) and APC-conjugated anti-MIP1β (clone 24006; RnD Systems) was

performed on ice for 1 hr. Samples were analyzed on a four-laser Fortessa flow cytometer (BD Biosciences). Data analysis was performed using FlowJo software (TreeStar, Ashland, OR) and positive populations were determined by a combination of fluorescence minus one (FMOs) and isotype controls.

Isolation of primary human monocytes

For cytokine assays, healthy donors were recruited anonymously through the Volunteer Blood Donor Registry. All subjects provided informed written consent, and were self-reported as being malaria naïve. Samples of 100 ml of whole blood were collected into K_2EDTA Vacutainer tubes (BD Biosciences) and processed within 2 hr of collection. For RNA-seq experiments, buffy packs were obtained from the Australian Red Cross, and processed within 24 hr of collection. The study was approved by the human ethics committee at the Walter and Eliza Hall Institute (project no. 13/06).

PBMC were purified from whole blood or buffy packs by Lymphoprep gradient centrifugation (D'Ombrain et al., 2007). Monocytes were enriched using isosmotic Percoll (GE Healthcare) density barrier centrifugation as described (de Almeida, Silva, Barral, & Barral Netto, 2000). Briefly, isosmotic Percoll solution (nine parts Percoll to one part NaCl 1.5 M) was mixed 1: (v/v) with PBS/citrate (NaH_2PO_4 1.49 mM; Na_2HPO_4 9.15 mM; NaCl 139.97 mM; $C_6H_5Na_3O_7$.$2H_2O$ 13mM; pH 7.2). Freshly isolated PBMC (5 ml at 1-2 x 10^7 cells/ml in PBS) was overlaid on 9 ml isosmotic Percoll/PBS/citrate solution in 15 ml centrifuge tubes, and centrifuged at 400 x g for 35 min. Monocytes at the PBS-Percoll interphase were collected and

washed twice with PBS before culturing in medium (RPMI-1640, 2 mM L-glutamine, 25 µM HEPES, 100 U/ml penicillin and 100 µg/ml streptomycin) supplemented with 10% FCS. Monocyte purity was verified by CD14 surface staining (CD14-FITC, clone M5E2; BD) and analysed on a FACS Calibur. Purity was on average ~80% (range 75-95%). For RNA-seq experiments, monocytes were further purified by FACS sorting gating on monocytes based on forward and side scatter. After sorting, monocyte purity was ≥99%.

Monocyte stimulation with parasite-derived vesicles

Tightly synchronized parasites at a minimum of 5% parasitemia, or uRBC control, were incubated at 4% hematocrit in 0.5% Albumax parasite medium for 12 hr prior to supernatant collection and vesicle purification. For uRBC control, fresh uRBC were washed in RPMI-HEPES and incubated at 37°C for 48 hr prior to setting up for vesicle collection. Vesicle preparations were maintained endotoxin-free to exclude potential non-specific responses. Monocytes from naïve Melbourne donors were added to triplicate wells in 96-well U-bottom plates at 2 x 10^5 cells/well, and stimulated with vesicles (5 µg/ml), or LPS positive control (3.5 ng/ml), for 12 hr at 37°C in 5% CO_2. In some instances, monocytes were also stimulated with 6 x 10^5 cells/well uRBC or iRBC. After incubation, plates were centrifuged and cell-free supernatants were collected and stored at -80°C until ready for use.

Multiplex cytokine/chemokine ELISA

Cell culture supernatants from stimulated monocytes (triplicate wells) were pooled and tested in duplicate. Multiplex ELISA (Bio-Plex Pro Assay; Bio-Rad) on a Luminex platform was performed according to manufacturer's instructions.

Library preparation and transcriptome sequencing

Human primary monocytes from 6 donors were isolated and stimulated with vesicles as described above for 6 hr. RNA was extracted using RNeasy Plus Kit (Qiagen) according to manufacturer's instructions. RNA and cDNA were quantified using the Agilent Tapestation and the Qubit DNA BR assay kit for Qubit 3.0 Fluorometer (Life technologies). An input of 100 ng of total RNA were prepared and indexed separately for sequencing using the TruSeq RNA sample Prep Kit (Illumina) as per manufacturer's instruction. Each library was quantified, and the indexed libraries were pooled and diluted to 1.5 pM for paired end sequencing on a NextSeq 500 generating 75 base pair paired end reads, using the v2 150 cycle High Output kit (Illumina) as per manufacturer's instructions.

Gene expression analysis

All samples were aligned to the human genome (GRCh38) using the Rsubread aligner (Liao, Smyth, & Shi, 2013), where greater than 90% of reads mapped in all samples. The number of fragments overlapping each Entrez gene were summarized using featureCounts (Liao, Smyth, & Shi, 2014) and NCBI RefSeq annotation (ftp://ftp.ncbi.nlm.nih.gov/gene/DATA/GENE_INFO/). Differential expression analyses were undertaken using the edgeR (McCarthy, Chen, & Smyth, 2012) and limma (Ritchie et al., 2015) software packages. Any gene which did not

achieve a count per million mapped reads (CPM) of 2 in at least 6 samples was deemed to be unexpressed and subsequently filtered from the analysis. Additionally, all genes without current annotation were also removed. Compositional differences between libraries were normalized using the trimmed mean of log expression ratios method (Robinson & Oshlack, 2010). Counts were transformed to $\log_2$-CPM with associated precision weights using voom (Law, Chen, Shi, & Smyth, 2014). Sample specific quality weights were also calculated using limma's arrayWeights function (Liu et al., 2015). Differential expression was assessed using linear models and robust empirical Bayes moderated t-statistics (Phipson, Lee, Majewski, Alexander, & Smyth, 2016). P-values were adjusted to control the false discovery rate (FDR) below 5% using the Benjamini and Hochberg method. To increase precision, the linear models incorporate 4 surrogate variables. These variables adjust the data for two know batch effects – donor and day of sample preparation (Figure S4). They were computed using limma's wsva function with weight.by.sd set to true.

Gene ontology (GO) pathway analyses used the limma goana function. To make the heatmap and multi-dimension scaling plot, the expression of each gene was summarised as a $\log_2$-CPM with a prior count of 2. These values were then adjusted using limma's removeBatchEffect function to incorporate the surrogate variable correction. The plots were made with limma's coolmap and plotMDS functions respectively. To reduce redundancy in GO terms, the REVIGO program (Supek, Bošnjak, Škunca, & Šmuc, 2011) was applied.

To identify any *Plasmodium falciparum* RNA in the samples, an index was built using the Rsubread package (Liao et al., 2013) that contained both the human and *falciparum* genomes (assemblies GRCh38 and *P. falciparum* 3D7 respectively).

All samples were then aligned to the combined genome using the Rsubread aligner. The number of reads aligning to *P. falciparum* chromosomes was quantified using featureCounts from Rsubread.

Acknowledgements

We thank Alan Cowman for providing the genetically modified parasite strains. We also thank Justin Boddey for kindly providing the Plasmepsin V antibody and Jake Baum for kindly providing the *Plasmodium falciparum* aldolase and ADF1 antibodies. RNA sequencing was performed at the WEHI Genome Hub with technical assistance from Stephen Wilcox.

Funding

This work was supported by National Health and Medical Research Council (NHMRC) grants APP106722 and APP1126395. N.G.S was supported by a NHMRC Dora Lush Scholarship [APP1038030]. This work was made possible through the Victorian State Government Operational Infrastructure Support and Australian Government NHMRC Independent Research Institute Infrastructure Support Scheme.

References

Aung, T., Chapuy, B., Vogel, D., Wenzel, D., Oppermann, M., Lahmann, M., . . . Wulf, G. G. (2011). Exosomal evasion of humoral immunotherapy in aggressive B-cell lymphoma modulated by ATP-binding cassette transporter A3. *Proceedings of the National Academy of Sciences, 108*(37), 15336-15341. doi:10.1073/pnas.1102855108

Aurrecoechea, C., Brestelli, J., Brunk, B. P., Dommer, J., Fischer, S., Gajria, B., . . . Wang, H. (2009). PlasmoDB: a functional genomic database for malaria parasites. *Nucleic Acids Research, 37*, D539-D543. doi:10.1093/nar/gkn814

Baruch, D. I., Gormely, J. A., Ma, C., Howard, R. J., & Pasloske, B. L. (1996). Plasmodium falciparum erythrocyte membrane protein 1 is a parasitized erythrocyte receptor for adherence to CD36, thrombospondin, and intercellular adhesion molecule 1. *Proceedings of the National Academy of Sciences of the United States of America, 93*(8), 3497-3502.

Baum, J., Richard, D., Healer, J., Rug, M., Krnajski, Z., Gilberger, T. W., . . . Cowman, A. F. (2006). A conserved molecular motor drives cell invasion and gliding motility across malaria life cycle stages and other apicomplexan parasites. *Journal of Biological Chemistry, 281*(8), 5197-5208. doi: 10.1074/jbc.M509807200

Beauvillain, C., Ruiz, S., Guiton, R., Bout, D., & Dimier-Poisson, I. (2007). A vaccine based on exosomes secreted by a dendritic cell line confers protection against T. gondii infection in syngeneic and allogeneic mice. *Microbes and Infection, 9*(14), 1614-1622. doi:10.1016/j.micinf.2007.07.002

Boddey, J. A., Hodder, A. N., Gunther, S., Gilson, P. R., Patsiouras, H., Kapp, E. A., . . . Cowman, A. F. (2010). An aspartyl protease directs malaria effector

proteins to the host cell. *Nature, 463*(7281), 627-631. doi:10.1038/nature08728

Buck, A. H., Coakley, G., Simbari, F., McSorley, H. J., Quintana, J. F., Le Bihan, T., . . . Maizels, R. M. (2014). Exosomes secreted by nematode parasites transfer small RNAs to mammalian cells and modulate innate immunity. *Nature Communications, 5*, 5488. doi:10.1038/ncomms6488

Bull, P. C., Lowe, B. S., Kortok, M., Molyneux, C. S., Newbold, C. I., & Marsh, K. (1998). Parasite antigens on the infected red cell surface are targets for naturally acquired immunity to malaria. *Nature Medicine, 4*(3), 358-360.

Cestari, I., Ansa-Addo, E., Deolindo, P., Inal, J. M., & Ramirez, M. I. (2012). Trypanosoma cruzi immune evasion mediated by host cell-derived microvesicles. *The Journal of Immunology, 188*(4), 1942-1952. doi:10.4049/jimmunol.1102053

Cooke, B. M., Buckingham, D. W., Glenister, F. K., Fernandez, K. M., Bannister, L. H., Marti, M., . . . Coppel, R. L. (2006). A Maurer's cleft-associated protein is essential for expression of the major malaria virulence antigen on the surface of infected red blood cells. *The Journal of Cell Biology, 172*(6), 899-908. doi:10.1083/jcb.200509122

Couper, K. N., Barnes, T., Hafalla, J. C. R., Combes, V., Ryffel, B., Secher, T., . . . de Souza, J. B. (2010). Parasite-derived plasma microparticles contribute significantly to malaria infection-induced inflammation through potent macrophage stimulation. *PLoS Pathogens, 6*(1), e1000744. doi:10.1371/journal.ppat.1000744

Cox, J., & Mann, M. (2008). MaxQuant enables high peptide identification rates, individualized p.p.b.-range mass accuracies and proteome-wide protein

quantification. *Nature Biotechnology, 26*(12), 1367-1372. doi:10.1038/nbt.1511

D'Ombrain, M. C., Robinson, L. J., Stanisic, D. I., Taraika, J., Bernard, N., Michon, P., . . . Schofield, L. (2008). Association of early interferon-gamma production with immunity to clinical malaria: a longitudinal study among Papua New Guinean children. *Clinical Infectious Diseases, 47*(11), 1380-1387. doi:10.1086/592971

D'Ombrain, M. C., Voss, T. S., Maier, A. G., Pearce, J. A., Hansen, D. S., Cowman, A. F., & Schofield, L. (2007). Plasmodium falciparum Erythrocyte Membrane Protein-1 Specifically Suppresses Early Production of Host Interferon-γ. *Cell Host and Microbe, 2*(2), 130-138. doi:10.1016/j.chom.2007.06.012

de Almeida, M. C., Silva, A. C., Barral, A., & Barral Netto, M. (2000). A simple method for human peripheral blood monocyte isolation. *Memórias do Instituto Oswaldo Cruz, 95*(2), 221-223.

De Maio, A. (2011). Extracellular heat shock proteins, cellular export vesicles, and the Stress Observation System: A form of communication during injury, infection, and cell damage: It is never known how far a controversial finding will go! Dedicated to Ferruccio Ritossa. *Cell Stress & Chaperones, 16*(3), 235-249. doi:10.1007/s12192-010-0236-4

Díaz Lozano, I. M., De Pablos, L. M., Longhi, S. A., Zago, M. P., Schijman, A. G., & Osuna, A. (2017). Immune complexes in chronic Chagas disease patients are formed by exovesicles from Trypanosoma cruzi carrying the conserved MASP N-terminal region. *Scientific Reports 7*, 44451. doi:10.1038/srep44451

Diaz, S. A., Martin, S. R., Grainger, M., Howell, S. A., Green, J. L., & Holder, A. A. (2014). Plasmodium falciparum aldolase and the C-terminal cytoplasmic

domain of certain apical organellar proteins promote actin polymerization. *Molecular and Biochemical Parasitology, 197*(1-2), 9-14. doi:10.1016/j.molbiopara.2014.09.006

Eriksson, E. M., Sampaio, N. G., & Schofield, L. (2013). Toll-Like Receptors and Malaria – Sensing and Susceptibility. *Journal of Tropical Diseases, 2*(1), 126-132. doi:10.4172/2329-891X.1000126

Gastpar, R., Gehrmann, M., Bausero, M. A., Asea, A., Gross, C., Schroeder, J. A., & Multhoff, G. (2005). Heat shock protein 70 surface-positive tumor exosomes stimulate migratory and cytolytic activity of natural killer cells. *Cancer Research, 65*(12), 5238-5247. doi:10.1158/0008-5472.can-04-3804

Gazzinelli, R. T., Kalantari, P., Fitzgerald, K. A., & Golenbock, D. T. (2014). Innate sensing of malaria parasites. *Nature Reviews Immunology, 14*(11), 744-757. doi:10.1038/nri3742

Goodyer, I. D., Johnson, J., Eisenthal, R., & Hayes, D. J. (1994). Purification of mature-stage Plasmodium falciparum by gelatine flotation. *Annals of Tropical Medicine and Parasitology, 88*(2), 209-211.

Jensen, A. T. R., Magistrado, P., Sharp, S., Joergensen, L., Lavstsen, T., Chiucchiuini, A., . . . Theander, T. G. (2004). Plasmodium falciparum associated with severe childhood malaria preferentially expresses PfEMP1 encoded by group A var genes. *The Journal of Experimental Medicine, 199*(9), 1179-1190. doi:10.1084/jem.20040274

Kriek, N., Tilley, L., Horrocks, P., Pinches, R., Elford, B. C., Ferguson, D. J. P., . . . Newbold, C. I. (2003). Characterization of the pathway for transport of the cytoadherence-mediating protein, PfEMP1, to the host cell surface in malaria parasite-infected erythrocytes. *Molecular Microbiology, 50*(4), 1215-1227.

Lässer, C., Eldh, M., & Lötvall, J. (2012). Isolation and characterization of RNA-containing exosomes. *Journal of visualized experiments 9*(59), e3037. doi:10.3791/3037

Law, C. W., Chen, Y., Shi, W., & Smyth, G. K. (2014). Voom: precision weights unlock linear model analysis tools for RNA-seq read counts. *Genome Biology, 15*(2), R29. doi:10.1186/gb-2014-15-2-r29

Liao, Y., Smyth, G. K., & Shi, W. (2013). The Subread aligner: fast, accurate and scalable read mapping by seed-and-vote. *Nucleic Acids Research, 41*(10), e108-e108. doi:10.1093/nar/gkt214

Liao, Y., Smyth, G. K., & Shi, W. (2014). FeatureCounts: an efficient general purpose program for assigning sequence reads to genomic features. *Bioinformatics, 30*(7), 923-930. doi:10.1093/bioinformatics/btt656

Liu, R., Holik, A. Z., Su, S., Jansz, N., Chen, K., Leong, H. S., . . . Ritchie, M. E. (2015). Why weight? Modelling sample and observational level variability improves power in RNA-seq analyses. *Nucleic Acids Research, 43*(15), e97-e97. doi:10.1093/nar/gkv412

Llinás, M., Bozdech, Z., Wong, E. D., Adai, A. T., & DeRisi, J. L. (2006). Comparative whole genome transcriptome analysis of three Plasmodium falciparum strains. *Nucleic Acids Research, 34*(4), 1166-1173. doi:10.1093/nar/gkj517

Lv, L.-H., Wan, Y.-L., Lin, Y., Zhang, W., Yang, M., Li, G.-L., . . . Min, J. (2012). Anticancer drugs cause release of exosomes with heat shock proteins from human hepatocellular carcinoma cells that elicit effective natural killer cell antitumor responses in vitro. *Journal of Biological Chemistry, 287*(19), 15874-15885. doi:10.1074/jbc.M112.340588

Maier, A. G., Cooke, B. M., Cowman, A. F., & Tilley, L. (2009). Malaria parasite proteins that remodel the host erythrocyte. *Nature Reviews Microbiology, 7*(5), 341-354. doi:10.1038/nrmicro2110

Maier, A. G., Rug, M., O'Neill, M. T., Beeson, J. G., Marti, M., Reeder, J., & Cowman, A. F. (2007). Skeleton-binding protein 1 functions at the parasitophorous vacuole membrane to traffic PfEMP1 to the Plasmodium falciparum-infected erythrocyte surface. *Blood, 109*(3), 1289-1297. doi:10.1182/blood-2006-08-043364

Maier, A. G., Rug, M., O'Neill, M. T., Brown, M., Chakravorty, S., Szestak, T., . . . Cowman, A. F. (2008). Exported proteins required for virulence and rigidity of Plasmodium falciparum-infected human erythrocytes. *Cell, 134*(1), 48-61. doi:10.1016/j.cell.2008.04.051

Mantel, P.-Y., Hjelmqvist, D., Walch, M., Kharoubi-Hess, S., Nilsson, S., Ravel, D., . . . Marti, M. (2016). Infected erythrocyte-derived extracellular vesicles alter vascular function via regulatory Ago2-miRNA complexes in malaria. *Nature Communications, 7*, 12727. doi:10.1038/ncomms12727

Mantel, P.-Y., Hoang, A. N., Goldowitz, I., Potashnikova, D., Hamza, B., Vorobjev, I., . . . Marti, M. (2013). Malaria-infected erythrocyte-derived microvesicles mediate cellular communication within the parasite population and with the host immune system. *Cell Host and Microbe, 13*(5), 521-534. doi:10.1016/j.chom.2013.04.009

Mantel, P.-Y., & Marti, M. (2014). The role of extracellular vesicles in Plasmodium and other protozoan parasites. *Cellular microbiology, 16*(3), 344-354. doi:10.1111/cmi.12259

Martin-Jaular, L., Nakayasu, E. S., Ferrer, M., Almeida, I. C., & Del Portillo, H. A. (2011). Exosomes from Plasmodium yoelii-infected reticulocytes protect mice from lethal infections. *PloS One, 6*(10), e26588. doi:10.1371/journal.pone.0026588

McCarthy, D. J., Chen, Y., & Smyth, G. K. (2012). Differential expression analysis of multifactor RNA-Seq experiments with respect to biological variation. *Nucleic Acids Research, 40*(10), 4288-4297. doi:10.1093/nar/gks042

McMillan, P. J., Millet, C., Batinovic, S., Maiorca, M., Hanssen, E., Kenny, S., . . . Tilley, L. (2013). Spatial and temporal mapping of the PfEMP1 export pathway in Plasmodium falciparum. *Cellular Microbiology, 15*(8), 1401-1418. doi:10.1111/cmi.12125

Miller, L. H., Baruch, D. I., Marsh, K., & Doumbo, O. K. (2002). The pathogenic basis of malaria. *Nature, 415*(6872), 673-679. doi:10.1038/415673a

Montes de Oca, M., Kumar, R., Rivera, Fabian de L., Amante, Fiona H., Sheel, M., Faleiro, Rebecca J., . . . Engwerda, Christian R. (2016). Type I interferons regulate immune responses in humans with blood-stage Plasmodium falciparum infection. *Cell Reports, 17*(2), 399-412. doi:10.1016/j.celrep.2016.09.015

Nantakomol, D., Dondorp, A. M., Krudsood, S., Udomsangpetch, R., Pattanapanyasat, K., & Combes, V. (2011). Circulating red cell-derived microparticles in human malaria. *Journal of Infectious Diseases, 203(5) 700-706*. doi:10.1093/infdis/jiq104

Phipson, B., Lee, S., Majewski, I. J., Alexander, W. S., & Smyth, G. K. (2016). Robust hyperparameter estimation protects against hypervariable genes and

improves power to detect differential expression. *The Annals of Applied Statistics, 10*(2), 946-963. doi:10.1214/16-AOAS920

Rappsilber, J., Mann, M., & Ishihama, Y. (2007). Protocol for micro-purification, enrichment, pre-fractionation and storage of peptides for proteomics using StageTips. *Nature Protocols, 2*(8), 1896-1906.

Reeder, J. C., Cowman, A. F., Davern, K. M., Beeson, J. G., Thompson, J. K., Rogerson, S. J., & Brown, G. V. (1999). The adhesion of Plasmodium falciparum-infected erythrocytes to chondroitin sulfate A is mediated by P. falciparum erythrocyte membrane protein 1. *Proceedings of the National Academy of Sciences, 96*(9), 5198-5202. doi:10.1073/pnas.96.9.5198

Regev-Rudzki, N., Wilson, D. W., Carvalho, T. G., Sisquella, X., Coleman, B. M., Rug, M., . . . Cowman, A. F. (2013). Cell-Cell communication between malaria-infected red blood cells via exosome-like vesicles. *Cell, 153*(5), 1120-1133. doi:10.1016/j.cell.2013.04.029

Ritchie, M. E., Phipson, B., Wu, D., Hu, Y., Law, C. W., Shi, W., & Smyth, G. K. (2015). Limma powers differential expression analyses for RNA-sequencing and microarray studies. *Nucleic Acids Research, 43*(7), e47. doi:10.1093/nar/gkv007

Robbins, P. D., & Morelli, A. E. (2014). Regulation of immune responses by extracellular vesicles. *Nature Reviews Immunology, 14*(3), 195-208. doi:10.1038/nri3622

Robinson, M. D., & Oshlack, A. (2010). A scaling normalization method for differential expression analysis of RNA-seq data. *Genome Biology, 11*(3), R25. doi:10.1186/gb-2010-11-3-r25

Salzer, U., Hinterdorfer, P., Hunger, U., Borken, C., & Prohaska, R. (2002). Ca(++)-dependent vesicle release from erythrocytes involves stomatin-specific lipid rafts, synexin (annexin VII), and sorcin. *Blood, 99*(7), 2569-2577.

Sampaio, N. G., Cheng, L., & Eriksson, E. M. (2017). The role of extracellular vesicles in malaria biology and pathogenesis. *Malaria Journal, 16*(1), 245. doi:10.1186/s12936-017-1891-z

Sampaio, N. G., Eriksson, E. M., Schofield. L. (2017). *Plasmodium falciparum* PfEMP1 modulates monocyte/macrophage transcription factor activation, and cytokine and chemokine responses. *Infection and Immunity.* doi:10.1128/IAI.00447-17

Schofield, L., & Grau, G. E. (2005). Immunological processes in malaria pathogenesis. *Nature Reviews Immunology, 5*(9), 722-735. doi:10.1038/nri1686

Shonhai, A., Boshoff, A., & Blatch, G. L. (2007). The structural and functional diversity of Hsp70 proteins from Plasmodium falciparum. *Protein Science, 16*(9), 1803-1818. doi:10.1110/ps.072918107

Silverman, J. M., Clos, J., Horakova, E., Wang, A. Y., Wiesgigl, M., Kelly, I., . . . Reiner, N. E. (2010). Leishmania exosomes modulate innate and adaptive immune responses through effects on monocytes and dendritic cells. *The Journal of Immunology, 185*(9), 5011-5022. doi:10.4049/jimmunol.1000541

Stanisic, D. I., Cutts, J., Eriksson, E., Fowkes, F. J. I., Rosanas-Urgell, A., Siba, P., . . . Schofield, L. (2014). γδ T cells and CD14+ monocytes are predominant cellular sources of cytokines and chemokines associated with severe malaria. *Journal of Infectious Diseases, 210*(2), 295-305. doi:10.1093/infdis/jiu083

Supek, F., Bošnjak, M., Škunca, N., & Šmuc, T. (2011). REVIGO summarizes and visualizes long lists of gene ontology terms. *PloS One, 6*(7), e21800. doi:10.1371/journal.pone.0021800

Szempruch, A. J., Sykes, S. E., Kieft, R., Dennison, L., Becker, A. C., Gartrell, A., . . . Harrington, J. M. (2016). Extracellular vesicles from Trypanosoma brucei mediate virulence factor transfer and cause host anemia. *Cell, 164*(1-2), 246-257. doi:10.1016/j.cell.2015.11.051

Szklarczyk, D., Morris, J. H., Cook, H., Kuhn, M., Wyder, S., Simonovic, M., . . . von Mering, C. (2017). The STRING database in 2017: quality-controlled protein–protein association networks, made broadly accessible. *Nucleic Acids Research, 45*(Database issue), D362-D368. doi:10.1093/nar/gkw937

Tauro, B. J., Greening, D. W., Mathias, R. A., Ji, H., Mathivanan, S., Scott, A. M., & Simpson, R. J. (2012). Comparison of ultracentrifugation, density gradient separation, and immunoaffinity capture methods for isolating human colon cancer cell line LIM1863-derived exosomes. *Methods, 56*(2), 293-304. doi:10.1016/j.ymeth.2012.01.002

Tembo, D. L., Nyoni, B., Murikoli, R. V., Mukaka, M., Milner, D. A., Berriman, M., . . . Montgomery, J. (2014). Differential PfEMP1 expression is associated with cerebral malaria pathology. *PLoS Pathogens, 10*(12), e1004537. doi:10.1371/journal.ppat.1004537

Twu, O., de Miguel, N., Lustig, G., Stevens, G. C., Vashisht, A. A., Wohlschlegel, J. A., & Johnson, P. J. (2013). Trichomonas vaginalis exosomes deliver cargo to host cells and mediate host∶parasite interactions. *PLoS Pathogens, 9*(7), e1003482. doi:10.1371/journal.ppat.1003482

Tyanova, S., Temu, T., & Cox, J. (2016). The MaxQuant computational platform for mass spectrometry-based shotgun proteomics. *Nature Protocols, 11*(12), 2301-2319. doi:10.1038/nprot.2016.136

Tyanova, S., Temu, T., Sinitcyn, P., Carlson, A., Hein, M. Y., Geiger, T., . . . Cox, J. (2016). The Perseus computational platform for comprehensive analysis of (prote)omics data. *Nature Methods, 13*(9), 731-740. doi:10.1038/nmeth.3901

Van Deun, J., Mestdagh, P., Sormunen, R., Cocquyt, V., Vermaelen, K., Vandesompele, J., . . . Hendrix, A. (2014). The impact of disparate isolation methods for extracellular vesicles on downstream RNA profiling. *Journal of Extracellular Vesicles, 3*. doi:10.3402/jev.v3.24858

Vega, V. L., Rodríguez-Silva, M., Frey, T., Gehrmann, M., Diaz, J. C., Steinem, C., . . . De Maio, A. (2008). Hsp70 translocates into the plasma membrane after stress and is released into the extracellular environment in a membrane-associated form that activates macrophages. *The Journal of Immunology, 180*(6), 4299-4307. doi:10.4049/jimmunol.180.6.4299

Voss, T. S., Healer, J., Marty, A. J., Duffy, M. F., Thompson, J. K., Beeson, J. G., . . . Cowman, A. F. (2006). A var gene promoter controls allelic exclusion of virulence genes in Plasmodium falciparum malaria. *Nature, 439*(7079), 1004-1008. doi:10.1038/nature04407

Wessel, D., & Flügge, U. I. (1984). A method for the quantitative recovery of protein in dilute solution in the presence of detergents and lipids. *Analytical Biochemistry, 138*(1), 141-143.

White, N. J., Pukrittayakamee, S., Hien, T. T., Faiz, M. A., Mokuolu, O. A., & Dondorp, A. M. (2014). Malaria. *The Lancet, 383*(9918), 723-735. doi:10.1016/S0140-6736(13)60024-0

Wong, W., Skau, C. T., Marapana, D. S., Hanssen, E., Taylor, N. L., Riglar, D. T., . . . Baum, J. (2011). Minimal requirements for actin filament disassembly revealed by structural analysis of malaria parasite actin-depolymerizing factor 1. *Proceedings of the National Academy of Sciences, 108*(24), 9869-9874. doi:10.1073/pnas.1018927108

Wong, W., Webb, A. I., Olshina, M. A., Infusini, G., Tan, Y. H., Hanssen, E., . . . Baum, J. (2014). A mechanism for actin filament severing by malaria parasite actin depolymerizing factor 1 via a low affinity binding interface. *Journal of Biological Chemistry, 289*(7), 4043-4054. doi:10.1074/jbc.M113.523365

Table 1 – Top twenty identified proteins in iRBC vesicle preparations by peptide count

Protein IDs	Protein name	Unique peptide count
Plasmodium falciparum protein		
PF3D7_0930300.1	Merozoite surface protein 1	22
PF3D7_0929400.1	High molecular weight rhoptry protein 2	19
PF3D7_1357100.1	Elongation factor 1-alpha	17
PF3D7_0302500.1; PF3D7_0302200.1	Cytoadherence linked asexual protein 3.1; cytoadherence linked asexual protein 3.2	11
PF3D7_0818900.1	Heat shock protein 70; heat shock protein 70	11
PF3D7_0915400.1	ATP-dependent 6-phosphofructokinase	11
PF3D7_0727400.1	Proteasome subunit alpha type-5, putative	10
PF3D7_0917900.1	Heat shock protein 70	10
PF3D7_1462800.1	Glyceraldehyde-3-phosphate dehydrogenase	9
PF3D7_0608500.1	Proteasome subunit alpha type-2, putative	8
PF3D7_0708400.1	Heat shock protein 90	7
PF3D7_0922600.1	Glutamine synthetase, putative	7
PF3D7_1117700.1	GTP-binding nuclear protein RAN/TC4	7
PF3D7_1353800.1	Proteasome subunit alpha type-4, putative	7
PF3D7_1470900.1	Proteasome subunit beta type-2, putative	7
PF3D7_0317000.1	Proteasome subunit alpha type-3, putative	6
PF3D7_0803800.1	Proteasome subunit beta type-4	6
PF3D7_0905400.1	High molecular weight rhoptry protein 3	6
PF3D7_1015600.1	Heat shock protein 60	6
PF3D7_1444800.1	Fructose-bisphosphate aldolase	6
	Human proteins	
P02549	Spectrin alpha chain, erythrocytic 1	34
P55072	Transitional endoplasmic reticulum ATPase	24
P11277	Spectrin beta chain, erythrocytic	22
P04040	Catalase	18
P16157	Ankyrin-1	17
P01023	Alpha-2-macroglobulin	14
P02730	Band 3 anion transport protein	13
P27105	Erythrocyte band 7 integral membrane protein	12
P01024	Complement C3	11

P13798	Acylamino-acid-releasing enzyme	10
P04075	Fructose-bisphosphate aldolase A	9
P11171	Protein 4.1	9
P04406	Glyceraldehyde-3-phosphate dehydrogenase	8
P13716	Delta-aminolevulinic acid dehydratase	8
P25786	Proteasome subunit alpha type-1	8
P25789	Proteasome subunit alpha type-4	8
P28074	Proteasome subunit beta type-5	8
P60900	Proteasome subunit alpha type-6	8
O14818; Q8TAA3	Proteasome subunit alpha type-7; Proteasome subunit alpha type-7-like	7
P00352	Retinal dehydrogenase 1	7

Table 2 – Proteins quantitatively different between vesicles from 3D7-WT iRBC and vesicles 3D7-UpsC^{R} iRBC

Protein IDs	Protein names	Protein/gene acronym	GO annotation	Log Student's T-test p-value	Mean's Difference
		Plasmodium falciparum proteins			
PF3D7_0930300.1	Merozoite surface protein 1	MSP-1	Pathogenesis	3.30	1.57
PF3D7_1462800.1	Glyceraldehyde-3-phosphate dehydrogenase	GAPDH	glycolytic process	2.36	1.48
PF3D7_1368100.1	26S proteasome regulatory subunit RPN11, putative	RPN11	Ubiquitin-dependent protein catabolic process	1.62	1.38
PF3D7_0617900.1; PF3D7_0610400.1	Histone H3 variant; histone H3	H3	Chromosome organization	1.44	-1.13
PF3D7_1328100.1	Proteasome subunit beta type-7, putative	--	Ubiquitin-dependent protein catabolic process	1.37	1.51
		Human proteins			
P06737	Glycogen phosphorylase, liver form	GYPL	Glucose homeostasis; glycogen metabolic process	1.94	1.50
Q9H4G4	Golgi-associated plant pathogenesis-related protein 1	GLIPR2	Regulation of ERK1 and ERK2 cascade;	1.81	0.60
P02790	Hemopexin	HPX	Cellular iron ion homeostasis;	1.78	-1.49
P00338	L-lactate dehydrogenase A chain	LDHA	Glycolytic process;	1.62	0.27
Q99880; Q99879; Q99877; Q93079; Q8N257; Q5QNW6; Q16778; P62807;	Histone H2B (multiple types)	H2B	DNA binding	1.52	2.91

P58876; P57053; P33778; P23527; P06899; O60814; Q96A08					
Q99436	Proteasome subunit beta type-7	PSMB7	Proteasome-mediated ubiquitin-dependent protein catabolic process	1.48	-1.00
P13796; P13797	Plastin-2	LCP1/PLS3	Actin binding	1.44	0.95
	Protein disulfide-isomerase-like protein of the testis		Cell redox homeostasis	1.43	1.65
P16157	Ankyrin-1	ANK1	Cytoskeleton organization	1.42	-0.67
P11166	Solute carrier family 2, facilitated glucose transporter member 1	SLC2A1	Glucose transmembrane transporter activity	1.34	-0.57

GO annotation – main gene ontology biological process terms associated with the protein

Mean's difference - measure of difference in abundance between means as log-fold change, positive indicating increase, negative indicating decrease; cut-off for biologically meaningful difference set at Log-fold 2

Table 3. Total number of genes differentially expressed between monocytes treated with different vesicle stimulus.

	WT vs. uRBC	3D7-UpsC^{R} vs. uRBC	3D7-UpsC^{R} vs. WT
Not significant	*9942*	*9593*	*10123*
Significant	*181*	*530*	*0*
Upregulated	116	326	0
Downregulated	65	204	0

Table 4. Top 20 DE genes in response to 3D7-WT and 3D7-UpsC^{R} vesicle stimulation, compared to uRBC vesicles

Gene ID	Symbol	Gene description	Gene type/function	Log FC	Adj. p-value
		3D7-WT vs. uRBC			
26118	WSB1	WD repeat and SOCS box containing 1	Ubiquitination	0.43	0.0062
905	CCNT2	cyclin T2	Transcription	0.35	0.0062
22797	TFEC	transcription factor EC	Transcription	0.31	0.0062
6142	RPL18A	ribosomal protein L18a	Translation	-0.37	0.0062
57018	CCNL1	cyclin L1	Translation	0.48	0.0062
6498	SKIL	SKI-like proto-oncogene	Transcription	0.27	0.0062
58487	CREBZF	CREB/ATF bZIP transcription factor	Transcription	0.35	0.0090
6168	RPL37A	ribosomal protein L37a	Translation	-0.23	0.0161
84449	ZNF333	zinc finger protein 333	Transcription	0.38	0.0184
54813	KLHL28	kelch like family member 28	Ubiquitination	0.29	0.0208
22107	ARL5B	ADP ribosylation factor like GTPase 5B	Intracellular signalling	0.28	0.0208
55023	PHIP	pleckstrin homology domain interacting protein	Intracellular signalling	0.32	0.0208
5339	PLEC	plectin	Cellular structure	0.22	0.0208
28546	CRIPAK	cysteine rich PAK1 inhibitor	Intracellular signalling	0.73	0.0208
40248	LINC01000	long intergenic non-protein coding RNA 1000	Non-coding RNA	0.46	0.0249
4637	MYL6	myosin light chain 6	Cell motility	-0.20	0.0249
7072	TIA1	TIA1 cytotoxic granule-associated RNA binding protein	Transcription	0.38	0.0249
72921	LOC72921	uncharacterized LOC729218	Unknown	0.44	0.0249
64089	SNX16	sorting nexin 16	Intracellular trafficking	0.32	0.0249
11480	MYSM1	Myb like, SWIRM and MPN domains 1	Transcription	0.33	0.0253
		3D7-UpsC^{R} vs. uRBC			
58487	CREBZF	CREB/ATF bZIP transcription factor	Transcription	0.56	0.0009
6498	SKIL	SKI-like proto-oncogene	Transcription	0.41	0.0009
26118	WSB1	WD repeat and SOCS box containing 1	Ubiquitination	0.59	0.0009
57018	CCNL1	cyclin L1	Translation	0.69	0.0009

55015	PRPF39	pre-mRNA processing factor 39	Translation	0.66	0.0009
22797	TFEC	transcription factor EC	Transcription	0.41	0.0013
13087	AHSA2	AHA1, activator of heat shock 90kDa protein	Intracellular trafficking	0.98	0.0013
2		ATPase homolog 2 (yeast)			
905	CCNT2	cyclin T2	Transcription	0.46	0.0013
2744	GLS	glutaminase	Metabolism	0.39	0.0016
64089	SNX16	sorting nexin 16	Intracellular trafficking	0.51	0.0016
10061	MIR5047	microRNA 5047	Non-coding RNA	0.90	0.0016
6408					
10011	TMEM170	transmembrane protein 170B	Unknown	0.38	0.0016
3407	B				
7072	TIA1	TIA1 cytotoxic granule-associated RNA binding	Transcription	0.59	0.0017
		protein			
51747	LUC7L3	LUC7 like 3 pre-mRNA splicing factor	Translation	0.65	0.0020
1958	EGR1	early growth response 1	Trancription	-0.99	0.0020
54540	FAM193B	family with sequence similarity 193 member B	Unknown	0.70	0.0020
79982	DNAJB14	DnaJ heat shock protein family (Hsp40) member	Intracellular trafficking	0.45	0.0021
		B14			
54813	KLHL28	kelch like family member 28	Ubiquitination	0.40	0.0022
64859	NABP1	nucleic acid binding protein 1	DNA repair	0.42	0.0022
50999	TMED5	transmembrane p24 trafficking protein 5	Intracellular signaling	0.39	0.0022

Genes in blue were enriched by both 3D7-WT and 3D7-UpsC^{R} EV treatment

Table 5. Top 20 enriched gene ontology terms enriched in response to 3D7-WT and 3D7-UpsC^{R} vesicle stimulation, compared to uRBC vesicles

GO term ID	Description	log10 p-value
	3D7-WT vs. uRBC	
GO:0070972	protein localization to endoplasmic reticulum	-18.26
GO:0000184	nuclear-transcribed mRNA catabolic process, nonsense-mediated decay	-16.60
GO:0019083	viral transcription	-15.44
GO:0044033	multi-organism metabolic process	-14.22
GO:0006413	translational initiation	-13.65
GO:0006364	rRNA processing	-12.94
GO:0046700	heterocycle catabolic process	-9.84
GO:0022613	ribonucleoprotein complex biogenesis	-8.99
GO:0061024	membrane organization	-8.63
GO:0034660	ncRNA metabolic process	-7.98
GO:1901566	organonitrogen compound biosynthetic process	-6.72
GO:0051704	multi-organism process	-6.57
GO:0043603	cellular amide metabolic process	-6.43
GO:0016071	mRNA metabolic process	-6.17
GO:1901564	organonitrogen compound metabolic process	-6.08
GO:0042590	antigen processing and presentation of exogenous peptide antigen via MHC class I	-5.49
GO:0009056	catabolic process	-5.41
GO:0006396	RNA processing	-5.11
GO:0044085	cellular component biogenesis	-4.95
GO:1901164	negative regulation of trophoblast cell migration	-4.36
	3D7-UpsC^{R} vs uRBC	
GO:0070972	protein localization to endoplasmic reticulum	-20.4881
GO:0019058	viral life cycle	-17.2899
GO:0006413	translational initiation	-15.3215
GO:0000184	nuclear-transcribed mRNA catabolic process, nonsense-mediated decay	-14.5452
GO:0046700	heterocycle catabolic process	-10.7375
GO:0006364	rRNA processing	-9.8601
GO:0051704	multi-organism process	-9.4023
GO:0006952	defense response	-9.2865
GO:0048002	antigen processing and presentation of peptide antigen	-8.9586

GO:0043603	cellular amide metabolic process	-7.8297
GO:0019882	antigen processing and presentation	-7.7447
GO:1901566	organonitrogen compound biosynthetic process	-7.4283
GO:0009056	catabolic process	-7.3134
GO:0061024	membrane organization	-7.163
GO:1901564	organonitrogen compound metabolic process	-7.1302
GO:0044763	single-organism cellular process	-7.0565
GO:0022613	ribonucleoprotein complex biogenesis	-6.7282
GO:0042221	response to chemical	-6.6596
GO:0071345	cellular response to cytokine stimulus	-6.3799
GO:0006950	response to stress	-6.3439

Terms in blue were enriched by both 3D7-WT and 3D7-UpsC^{R} EV treatment

GO term ID – gene ontology term identification number

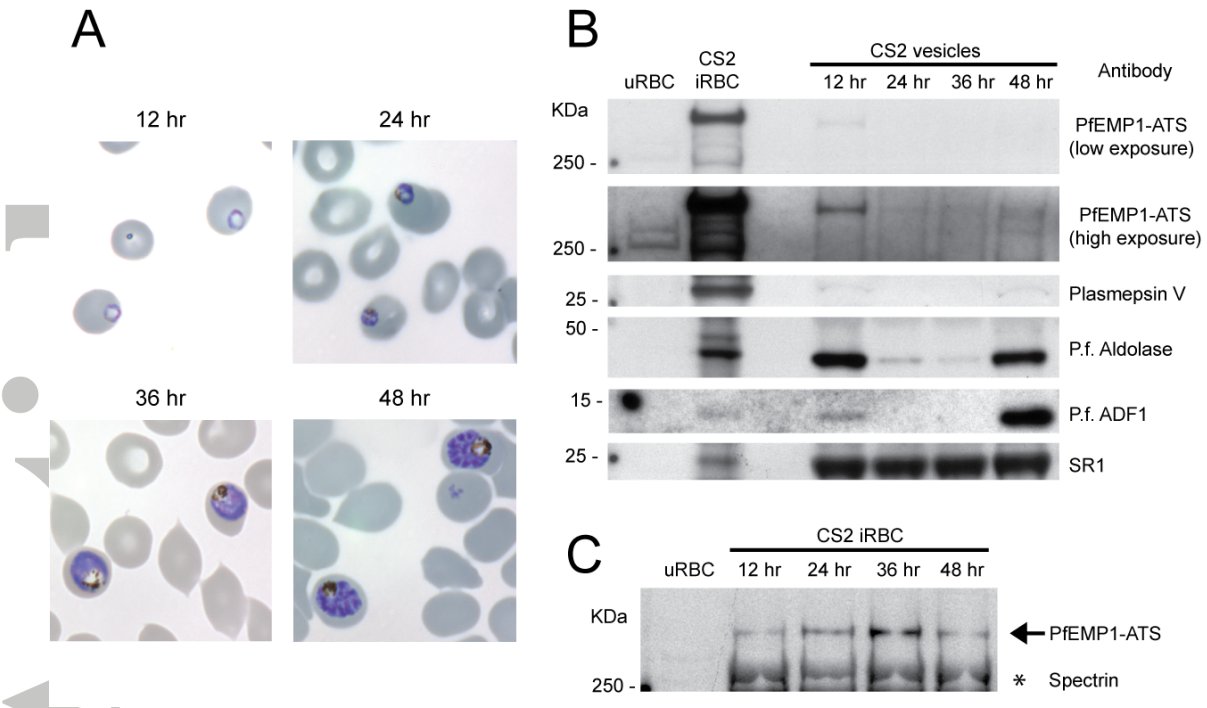

Figure 1. Variation in parasite protein content in vesicles from different iRBC life stages. CS2-infected iRBC were tightly synchronized and cell culture supernatants were collected at 0-12 hr, 12-24 hr, 24-36 hr, and 36-48 hr. A) Giemsa stain of parasite cultures at supernatant collection time. B) Lysates from uRBC, trophozoite-stage CS2 iRBC, and CS2 vesicles from culture supernatants collected at the specified time points, were analysed by Western Blot for indicated proteins. C) Lysates from uRBC or CS2 iRBC at the specified time points were analysed by Western blot; arrow indicates PfEMP1 and asterisk indicates cross-reactivity with human spectrin. Representative images of two independent repeats.

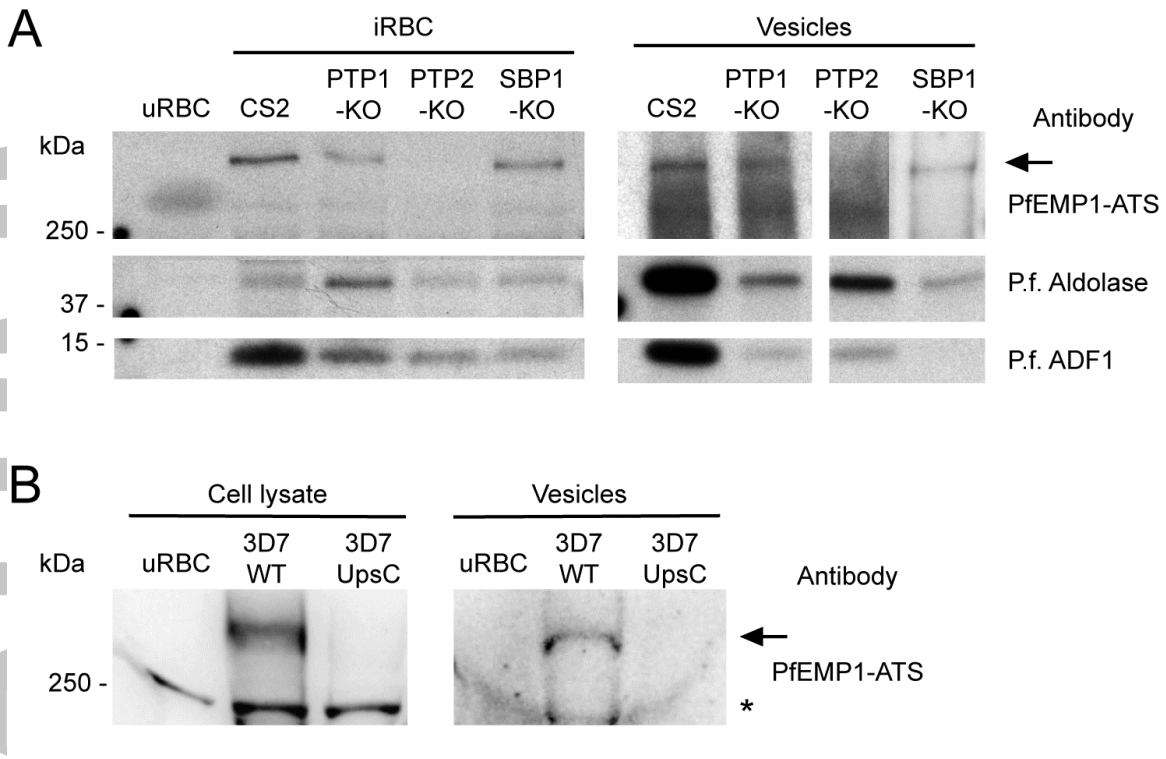

Figure 2. PfEMP1 in vesicles from PfEMP1 transport knock-out and PfEMP1 expression knock-out parasite strains. Lysates from uRBC/iRBC and ring-stage vesicles from PfEMP1 transport knock-out parasites PTP1-KO, PTP2-KO and SBP1-KO (A), and lysates and ring-stage vesicles from uRBC, 3D7-WT and PfEMP1 expression knock-out 3D7-UpsC^{R} (B) were analysed for expression of PfEMP1 and other parasite proteins by Western blot. Arrow indicates PfEMP1 and asterisk indicates cross-reactivity with human spectrin. Representative images of two independent repeats. Representative images of minimum two independent repeats.

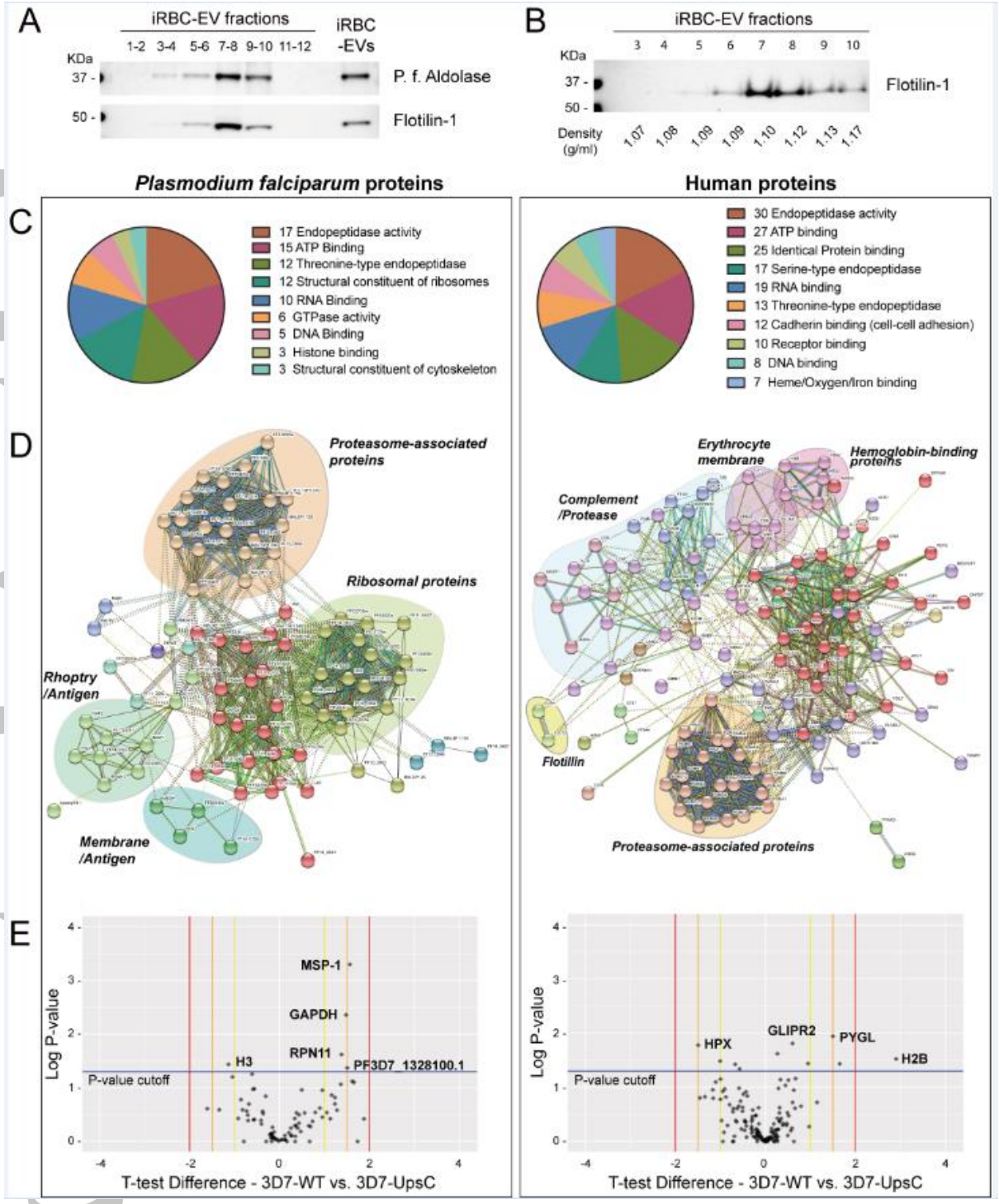

Figure 3. Proteomic analysis of protein content of vesicles from 3D7-WT and 3D7-UpsC^{R} iRBC. A) Cell culture supernatant from ring-stage 3D7-WT iRBC was fractionated by Optiprep density centrifugation, and fraction pairs were analysed by Western blot for *P. falciparum* aldolase and human exosome marker flotilin-1, compared to unfractionated vesicles. B) Fractions 3-10, prepared as in (A), were

analysed by Western blot for flotilin-1, and density of individual fractions was measured. C) Overarching molecular function gene ontologies of low stringency proteins identified by mass spectrometry analysis of vesicles from both 3D7-WT and 3D7-UpsC^{R} ring-stage iRBC, from fractions 7 and 8 of samples fractionated as in (A). Gene ontologies of both *Plasmodium falciparum* proteins (left) and human proteins (right) are shown. D) Protein interactome network for iRBC-EVs proteins identified from *Plasmodium* and human datasbases using the STRING software. Proteins nodes and interactions (direct/physical and indirect/functional represented by continuous and interrupted lines, respectively) are coloured according to MCL clustering. E) Volcano plots of quantitative analysis of proteins in vesicles from 3D7-WT vs. 3D7-UpsC^{R}, showing log-fold change t-test difference in the x-axis and log-P-value in the y-axis. Blue horizontal line indicates cut-off for P=0.05, and yellow, orange, and red vertical lines indicate means difference log-fold of 1, 1.5, and 2, respectively. Quantitation of both *Plasmodium falciparum* proteins (left) and human proteins (right) are shown. Three biological replicates were used for mass spectrometry analysis in (C) and (D).

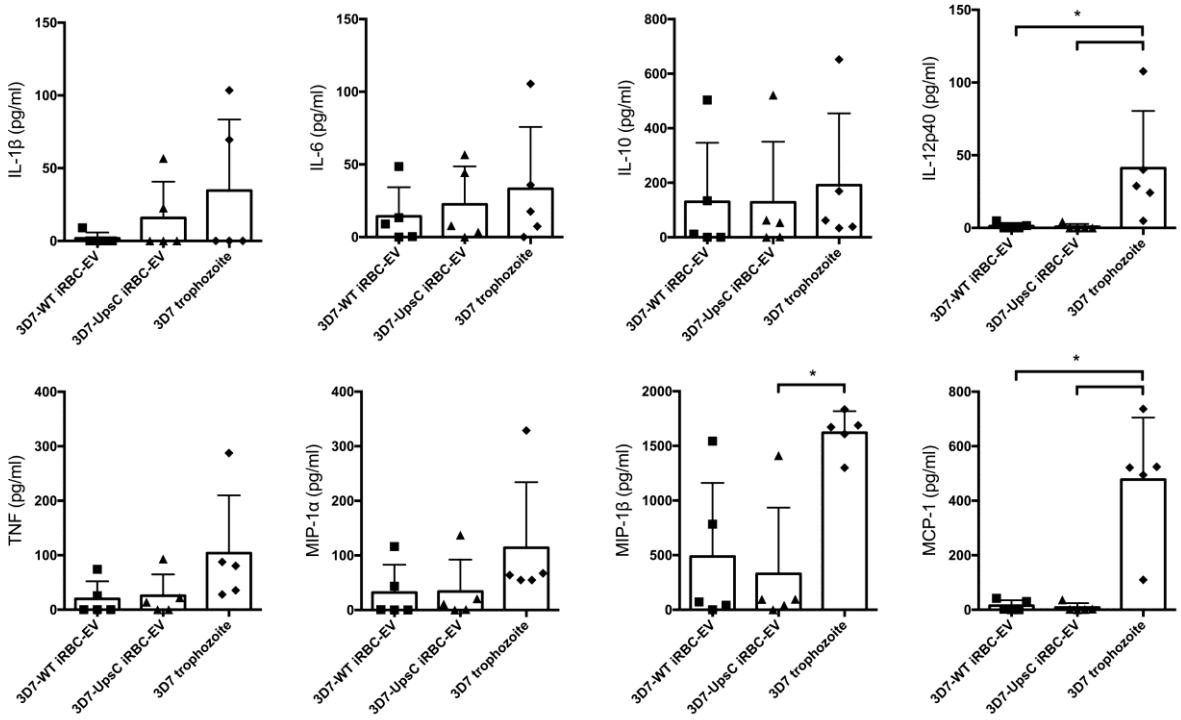

Figure 4. Monocyte cytokine responses to stimulus with parasite vesicles and iRBC. Naïve primary human monocytes (n=5 donors) were negatively isolated and stimulated for 12 hr with 5 µg/ml of vesicles from uRBC, 3D7-WT or 3D7-UpsC^{R} iRBC, or whole intact uRBC or 3D7-WT trophozoites (ratio of 3 RBC/iRBC to 1 monocyte). Levels of indicated cytokines in the culture supernatant were measured by multiplex cytokine ELISA. Data shown is after subtraction of uRBC background from iRBC-stimulated samples. Two-way ANOVA, * indicates $P<0.05$.

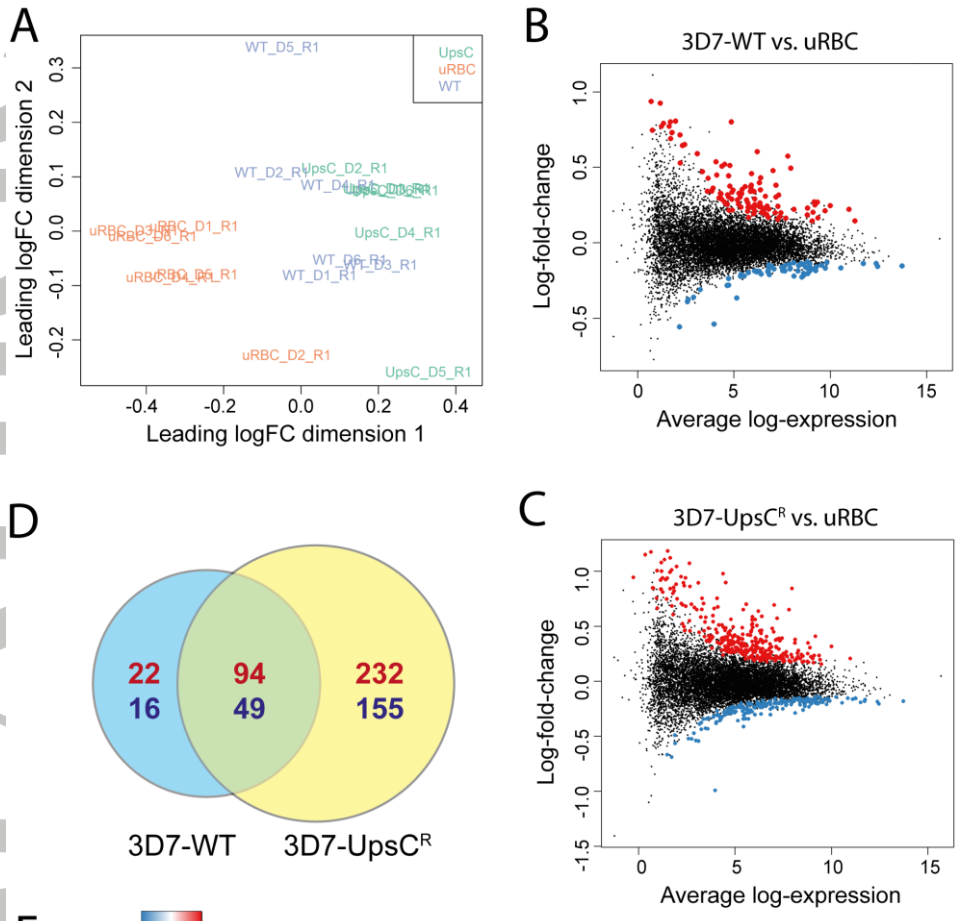

Figure 5. RNA-sequencing of monocytes stimulated with vesicles from uRBC, 3D7-WT iRBC and 3D7-UpsC^{R} iRBC. Naïve primary human monocytes (n=6 donors) were negatively isolated and stimulated for 6 hr with 5 µg/ml of vesicles from uRBC, 3D7-WT or 3D7-UpsC^{R} iRBC, prior to RNA extraction and RNA-sequencing. A) Multi-dimensional scaling plot after correction for donor and experimental day effects. Samples in orange, mauve, and green represent uRBC, 3D7-WT, and 3D7-UpsC^{R} vesicles stimulated samples, respectively. B) Mean-difference plot of average log-expression for each gene (x-axis) against their log-fold change (y-axis) for 3D7-WT vs. uRBC, C) and 3D7-UpsC^{R} vs. uRBC. The deferentially expressed genes are highlighted, with points coloured in red and blue indicating up- and down-regulated genes respectively. D) Venn diagram of number of up-regulated (red) and down-regulated (blue) genes in common between monocytes stimulated with vesicles from 3D7-WT vs. uRBC and 3D7-UpsC^{R} vs. uRBC. E) Heatmap of the expression of the 530 DE genes between 3D7-UpsC^{R} and uRBC. The Z-scores are batch corrected log-CPM (counts per million) scaled to have mean 0 and standard deviation. Genes are displayed horizontally for each donor (1-6), and stimulus condition (uRBC, 3D7-WT, or 3D7-UpsC^{R} vesicles) labelled in the bottom. The red and blue colouring indicates increased and decreased expression respectively.